

CERN-EP-2024-230
12 September 2024

Measurement of the effective leptonic weak mixing angle

LHCb collaboration[†]

Abstract

Using pp collision data at $\sqrt{s} = 13$ TeV, recorded by the LHCb experiment between 2016 and 2018 and corresponding to an integrated luminosity of 5.4 fb^{-1} , the forward-backward asymmetry in the $pp \rightarrow Z/\gamma^* \rightarrow \mu^+\mu^-$ process is measured. The measurement is carried out in ten intervals of the difference between the muon pseudorapidities, within a fiducial region covering dimuon masses between 66 and 116 GeV, muon pseudorapidities between 2.0 and 4.5 and muon transverse momenta above 20 GeV. These forward-backward asymmetries are compared with predictions, at next-to-leading order in the strong and electroweak couplings. The measured effective leptonic weak mixing angle is

$$\sin^2 \theta_{\text{eff}}^{\ell} = 0.23147 \pm 0.00044 \pm 0.00005 \pm 0.00023,$$

where the first uncertainty is statistical, the second arises from systematic uncertainties associated with the asymmetry measurement, and the third arises from uncertainties in the fit model used to extract $\sin^2 \theta_{\text{eff}}^{\ell}$ from the asymmetry measurement. This result is based on an arithmetic average of results using the CT18, MSHT20, and NNPDF31 parameterisations of the proton internal structure, and is consistent with previous measurements and with predictions from the global electroweak fit.

To be submitted to JHEP

© 2024 CERN for the benefit of the LHCb collaboration. [CC BY 4.0 licence](https://creativecommons.org/licenses/by/4.0/).

[†]Authors are listed at the end of this paper.

1 Introduction

The weak mixing angle θ_W is one of the fundamental parameters of the Standard Model; at lowest order it relates the values of the U(1) and SU(2) gauge couplings. Consequently, it controls the couplings of the Z boson: the tree-level vector coupling to an elementary fermion of charge Q and third weak-isospin component T_3 is $T_3 - 2Q \sin^2 \theta_W$. Higher-order corrections to the couplings are then included by defining an effective angle, which for leptons can be written via

$$\sin^2 \theta_{\text{eff}}^\ell \equiv \kappa_{\text{lept}} \sin^2 \theta_W, \quad (1)$$

where the factor κ_{lept} contains both universal and flavour-specific terms [1]. The weak mixing angle is scale dependent; we define $\sin^2 \theta_{\text{eff}}^\ell$ to be evaluated at a renormalisation scale equal to the mass of the Z boson. The value of $\sin^2 \theta_{\text{eff}}^\ell$ can be predicted by global electroweak fits [2, 3], and a comparison of these predictions to direct measurements is sensitive to possible corrections involving fields beyond those present in the Standard Model. This article reports a measurement of $\sin^2 \theta_{\text{eff}}^\ell$ using data collected with the LHCb detector at the Large Hadron Collider (LHC).

The two most precise measurements of $\sin^2 \theta_{\text{eff}}^\ell$ are from the forward-backward asymmetry in $e^+e^- \rightarrow Z \rightarrow b\bar{b}$ processes at LEP [1] and the leptonic coupling asymmetry at the SLD experiment [4]. These two results are in tension at the level of 3.2 standard deviations. Additional measurements have also been combined by the LEP experiments [1]. Measurements at hadron colliders have also been reported by the ATLAS [5], CMS [6] and LHCb [7] experiments at the LHC, and by the CDF and D0 experiments at the Tevatron [8].

At hadron colliders $\sin^2 \theta_{\text{eff}}^\ell$ can be determined from $Z \rightarrow \ell^+\ell^-$ production,¹ where ℓ is an electron or muon. The differential cross-section follows [9, 10]

$$\frac{d\sigma}{d\cos\theta^*} \propto 1 + \cos^2\theta^* + \alpha \cos\theta^*, \quad (2)$$

where θ^* is the polar angle in a suitable frame. In the Collins–Soper frame [9], θ^* can be calculated from variables in the laboratory frame via

$$\cos\theta^* = \frac{2(P_1^+ P_2^- - P_1^- P_2^+)}{\sqrt{m_{\ell\ell}^2(m_{\ell\ell}^2 + p_{T,\ell\ell}^2)}} \frac{p_{z,\ell\ell}}{|p_{z,\ell\ell}|}, \quad (3)$$

where $p_{T,\ell\ell}$, $p_{z,\ell\ell}$ and $m_{\ell\ell}$ are the transverse momentum, longitudinal momentum and mass of the dilepton system, respectively. The $P_i^\pm \equiv \frac{1}{\sqrt{2}}(E_i \pm p_{z,i})$ terms are calculated from the energies (E) and longitudinal momenta (p_z) of the lepton and antilepton, which are labelled with i values of 1 and 2, respectively. The final factor in Eq. 3, corresponding to the sign of $p_{z,\ell\ell}$, is required in proton-proton (pp) collisions given the symmetry of the initial state.

The coefficient α in Eq. 2 arises through terms involving products of vector and axial-vector couplings and can therefore be directly related to the weak mixing angle. In addition, since the relevant term in Eq. 2 is linear in $\cos\theta^*$ it also directly causes a forward-backward asymmetry in $Z \rightarrow \ell^+\ell^-$ production; measurements of this asymmetry

¹For brevity we use Z to refer to the physical process including amplitudes with Z and virtual photon propagators.

36 can then be used to determine $\sin^2 \theta_{\text{eff}}^\ell$. The forward-backward asymmetry is typically
 37 defined as

$$A_{\text{FB}} \equiv \frac{\sigma_{\text{F}} - \sigma_{\text{B}}}{\sigma_{\text{F}} + \sigma_{\text{B}}}, \quad (4)$$

38 where $\sigma_{\text{F,B}}$ are the cross-sections integrated over the ranges $0 < \cos \theta^* < 1$ (forward, F)
 39 and $-1 < \cos \theta^* < 0$ (backward, B). Since events with the largest values of $|\cos \theta^*|$ are
 40 most sensitive to the linear term in Eq. 2, these events also provide the greatest sensitivity
 41 to the weak mixing angle. Therefore, in some previous analyses [5, 6], the weak mixing
 42 angle has been extracted from an angular analysis or by measuring A_{FB} using a per-event
 43 weighting that depends on $\cos \theta^*$ [11]. In this paper we follow a related approach, by
 44 considering A_{FB} in intervals of the absolute difference between the pseudorapidities of
 45 the two muons produced in the Z boson decay, $|\Delta\eta|$. Since $\cos \theta^* \sim \tanh(\Delta\eta/2)$ [12] this
 46 choice enables us to separate the events with the greatest sensitivity to the weak mixing
 47 angle. In simulation this binning improves sensitivity to the weak mixing angle by 14 %
 48 when compared to an approach with no binning in $|\Delta\eta|$. For simplicity, following this
 49 binning choice, we also define ‘forward’ and ‘backward’ labels based on the sign of the
 50 difference in pseudorapidity of the muons. This is of negligible consequence: the assigned
 51 ‘forward’ or ‘backward’ label is different with this choice to that using the Collins–Soper
 52 angle for only one candidate Z decay in the analysis reported in this article. In summary,
 53 this analysis measures

$$A_{\text{FB}} \equiv \frac{N(\eta^- > \eta^+) - N(\eta^- < \eta^+)}{N(\eta^- > \eta^+) + N(\eta^- < \eta^+)}, \quad (5)$$

54 as a function of $|\Delta\eta|$, where N denotes a yield of events passing the requirements in
 55 parentheses corrected for detector effects, and η^- and η^+ are the pseudorapidities of the
 56 negatively and positively charged leptons, respectively.

57 This analysis uses pp collision data at a center-of-mass energy of 13 TeV, recorded
 58 with the LHCb detector during 2016, 2017 and 2018, and corresponding to an integrated
 59 luminosity of 5.4 fb^{-1} . The analysis is carried out in two parts. In the first stage A_{FB}
 60 is measured in ten intervals of $|\Delta\eta|$ up to $|\Delta\eta| = 2.5$, using $Z \rightarrow \mu^+\mu^-$ decays. The
 61 asymmetries are measured in the fiducial region corresponding to dimuon masses in the
 62 range $66 < M < 116 \text{ GeV}$, and with individual muon pseudorapidities in the range
 63 $2.0 < \eta < 4.5$ and transverse momenta $p_{\text{T}} > 20 \text{ GeV}$.² The second stage of the analysis
 64 compares the measurement with theoretical templates to determine $\sin^2 \theta_{\text{eff}}^\ell$. In order to
 65 prevent human bias, the analysis has been carried out by introducing an unknown offset
 66 in the $\sin^2 \theta_{\text{eff}}^\ell$ value until the analysis methodology was finalised.

67 2 Dataset

68 The LHCb detector [13, 14] is a single-arm forward spectrometer, which covers the
 69 pseudorapidity range $2 < \eta < 5$. The detector includes a high-precision tracking system
 70 consisting of a silicon-strip vertex detector surrounding the pp interaction region [15], a
 71 large-area silicon-strip detector (the TT) located upstream of a dipole magnet with a
 72 bending power of about 4 T m, and three stations of silicon-strip detectors and straw drift

²Throughout this paper we use natural units, where $c = 1$. We also define p_{T} , η and the dimuon invariant mass based on the stable final-state particles (commonly referred to as being measured at bare level).

73 tubes [16] placed downstream of the magnet. Roughly half of the data were recorded with
74 the magnet in each of the two polarity configurations. The tracking system provides a
75 measurement of the momentum, p , of charged particles with a relative uncertainty that
76 varies from 0.5% at low momentum to 1.0% at 200 GeV. The minimum distance of a track
77 to a primary pp collision vertex (PV) is referred to as the impact parameter (IP), which
78 is precisely determined by the vertex detector. Different types of charged hadrons are
79 distinguished using information from two ring-imaging Cherenkov detectors [17]. Photons,
80 electrons and hadrons are identified by a calorimeter system consisting of scintillating-pad
81 and preshower detectors, an electromagnetic calorimeter and a hadronic calorimeter.
82 Muons are identified by a system composed of alternating layers of iron and multiwire
83 proportional chambers [18].

84 This analysis uses events selected by the hardware trigger based on the presence of
85 a muon with a high transverse momentum. The software trigger performs a full event
86 reconstruction, and this analysis selects events based on the presence of high-transverse-
87 momentum muon candidates [19].

88 Simulation is required to model and correct for the effects of the detection efficiency
89 and resolution, and backgrounds. In the simulation, pp collisions are generated using
90 PYTHIA [20] with a specific LHCb configuration [21]. Decays of heavy particles such
91 as weak bosons, and top quarks, are modelled directly with PYTHIA, while decays of
92 lighter particles are described by EVTGEN [22], in which final-state radiation is generated
93 using PHOTOS [23]. The interaction of the generated particles with the detector, and its
94 response, are implemented using the GEANT4 toolkit [24] as described in Ref. [25].

95 Candidate $Z \rightarrow \mu^+\mu^-$ decays are formed from combinations of oppositely charged and
96 positively identified muons, with $p_T > 20$ GeV and $2 < \eta < 4.5$, and with dimuon invariant
97 masses between 66 and 116 GeV. After this initial selection the level of background is
98 already very low, but several additional requirements are imposed to further improve the
99 sample purity, with minimal reduction in the detection efficiency for the signal. Both
100 muons are required to have a small IP with respect to the relevant PV in order to suppress
101 background from heavy-flavour-hadron decays, and their corresponding track fits must
102 have χ^2 values below 2.5 to suppress hadronic backgrounds. The sum of the transverse
103 momenta of particles within $(\Delta\eta)^2 + (\Delta\phi)^2 < 0.4^2$ of each muon must be less than 40 GeV
104 (where ϕ denotes the azimuthal angle). This requirement suppresses hadronic backgrounds
105 since they typically have increased activity close to the muons. In order to precisely define
106 the trigger efficiency, each candidate is required to have at least one muon that satisfies
107 the requirements of the hardware and software triggers. After all these requirements
108 around 860 000 events are selected.

109 The decays $J/\psi \rightarrow \mu^+\mu^-$ and $\Upsilon(1S) \rightarrow \mu^+\mu^-$ are used to calibrate the detection
110 efficiency (discussed in detail in Sec. 3) and the muon momentum measurement. Candidates
111 for both decays are formed from combinations of oppositely charged tracks identified as
112 muons with $p_T > 3$ GeV. The $J/\psi \rightarrow \mu^+\mu^-$ candidates are required to form a vertex that
113 is significantly displaced from any PV; this implies that the signal originates from decays
114 of b hadrons.

115 Two calibrations are applied to the muon momenta in the data. The first is to
116 correct for gradual variations of the momentum scale with time, known to be at the
117 $\mathcal{O}(10^{-4})$ level [26]. Multiplicative correction factors are determined from the observed
118 variation of the $\Upsilon(1S) \rightarrow \mu^+\mu^-$ peak position in intervals of the data-taking period. The
119 second correction addresses charge-dependent curvature biases using the pseudomass

120 method [27, 28]. The pseudomass is an estimate of the mass of two-particle final states, in
 121 which the magnitude of one of the momenta is ignored. Considering the decay $Z \rightarrow \mu^+ \mu^-$
 122 we define the two pseudomasses:

$$\mathcal{M}^\pm \equiv \sqrt{2p^\pm p_T^\pm \frac{p^\mp}{p_T^\mp} (1 - \cos \vartheta)}, \quad (6)$$

123 where p^+ and p^- denote the magnitudes of the μ^+ and μ^- momenta (and similarly
 124 for the transverse momenta p_T^\pm), and ϑ is the opening angle between the two muons.
 125 Effectively, the pseudomass estimates the dimuon invariant mass under the assumption
 126 that Z bosons are produced with transverse momenta much smaller than their mass. For a
 127 perfectly aligned detector, we expect to a very good approximation that the \mathcal{M}^+ and \mathcal{M}^-
 128 distributions should agree. However, unlike the dimuon invariant mass, in which charge-
 129 dependent curvature biases strongly cancel, the pseudomasses have first-order sensitivity
 130 to these biases, thereby allowing these effects to be easily determined. In intervals of η , ϕ ,
 131 year and magnet polarity, a simultaneous fit of the positive and negative pseudomass is
 132 performed to find the pseudomass asymmetry. This is then directly translated to provide
 133 corrections for biases in measurements of the charge-over-momentum, q/p . The difference
 134 between the q/p biases found in data and simulation is then applied as a correction to
 135 data; this approach eliminates a small bias due to the presence of vector and axial-vector
 136 couplings in the physics process. It is shown comprehensively in Ref. [28] that this effect is
 137 both small, and has minimal dependence on the value of $\sin^2 \theta_{\text{eff}}^\ell$ assumed in the simulation.

138 3 Corrections to the simulation and background mod- 139 elling

140 The simulation is used to model the detection efficiency and backgrounds, and subsequently
 141 to correct the data for these contributions. Corrections to the simulation are required
 142 to improve the accuracy of this modelling, with systematic uncertainties then associated
 143 with these corrections.

144 Some of the effects contributing to the momentum resolution are underestimated in
 145 the simulation; smearing of the momenta in the simulation is therefore required. The
 146 approach taken here closely follows that in the LHCb measurement of the W boson
 147 mass [29], using selected J/ψ , $\Upsilon(1S)$ and Z -boson events. The information provided by
 148 each of these three resonances is complementary, due to the different average momenta of
 149 the muons produced. The impact of this smearing on the final result is negligible.

150 The detection efficiency for the $Z \rightarrow \mu^+ \mu^-$ signal is roughly 85%, with the main
 151 contributors to the inefficiency being the trigger, track reconstruction and muon iden-
 152 tification. Corrections are applied to the simulation in order to improve the accuracy
 153 with which the detection efficiency is modelled. The trigger efficiency is measured in
 154 both data and simulation using a combination of $Z \rightarrow \mu^+ \mu^-$ candidates, which provide
 155 constraints at high p_T , and $\Upsilon(1S) \rightarrow \mu^+ \mu^-$ candidates, which provide constraints at lower
 156 p_T . Candidates are required to have one muon that satisfies the requirements of the
 157 trigger; the other muon is therefore not required to trigger the recording of the event. In
 158 intervals of the direction of the other muon, the efficiency is estimated by the fraction of
 159 these candidates in which both muons satisfy the trigger requirements. Nine and four

160 intervals are simultaneously used in η and ϕ , respectively, and the efficiency estimates
 161 are further divided into intervals of p_T . In each angular interval, the p_T dependence of
 162 the efficiency in the simulation is modelled with an error function, while the ratio of the
 163 efficiency in data to that in simulation is modelled with a linear function. These functions
 164 are used to assign a weight to each simulated event, depending on whether one or both
 165 muons satisfy the trigger requirement.

166 The muon identification efficiency is determined in a similar way, using only $Z \rightarrow \mu^+\mu^-$
 167 candidates. A dedicated sample of $Z \rightarrow \mu^+\mu^-$ candidates is selected with one muon allowed
 168 to fail the muon identification requirements, while the other must match the standard
 169 requirement. The fraction of these candidates in which both muons satisfy the requirements
 170 provides an estimate of the efficiency. By comparing these estimates for the data and
 171 simulation, weights are assigned to the simulated events based on parametric functions of
 172 p_T , determined in intervals of η and ϕ .

173 The track reconstruction efficiency is also determined with a dedicated sample of
 174 $Z \rightarrow \mu^+\mu^-$ candidates in which one muon is reconstructed using only information from
 175 the TT and the muon subdetectors. The fraction of events in which the muon is also found
 176 by the standard track-reconstruction algorithms [30] provides an estimate of the efficiency.
 177 Corresponding weights are assigned to the simulated events. Unlike the trigger and muon
 178 identification, the tracking efficiency corrections have no significant p_T dependence for the
 179 high p_T muons studied.

180 The backgrounds in the $Z \rightarrow \mu^+\mu^-$ samples are modelled using simulation. The total
 181 background fraction, within the kinematic region in which A_{FB} is measured, is only 2×10^{-3} .
 182 Most backgrounds have steeply falling mass distributions, and are therefore relatively small
 183 in the region $66 < M < 116$ GeV. The two largest background contributions arise from
 184 $Z \rightarrow \tau^+\tau^-$ decays and from the decays of heavy-flavour hadrons. Both these contribute
 185 to the sample with fractions of around 5×10^{-4} . Contributions from rarer processes are
 186 also considered, including weak-boson pair production, top-quark pair production, single-
 187 top-quark production, the production of W bosons associated with hadrons misidentified
 188 as muons, and events with two hadrons misidentified as muons.

189 Figure 1 compares the dimuon invariant mass and $\Delta\eta$ distributions of the selected
 190 candidates in data to simulation that includes both signal and background contributions.
 191 Both distributions are well described by the simulation, and it can be seen that the
 192 background level is extremely low.

193 4 Measurement of the forward-backward asymmetry

194 The measurement of the forward-backward asymmetry proceeds by measuring the forward
 195 and backward yields in ten intervals of $|\Delta\eta|$ and finding A_{FB} following Eq. 5. Corrections
 196 are necessary to account for the presence of background and detector effects such as
 197 inefficiencies. Figure 2 shows the numerical effect of these two corrections. The background
 198 is modelled as described above, with the background yields directly subtracted from the
 199 forward and backward yields. This correction is seen to have a very small effect on the
 200 measured A_{FB} values. The correction for detector effects is typically at the $\mathcal{O}(10^{-4})$ level.
 201 Systematic effects of a few $\times 10^{-3}$ are seen in some intervals, though these are subject to
 202 larger statistical uncertainties due to the finite simulation sample sizes. We discuss the
 203 correction for detector effects in more detail below.

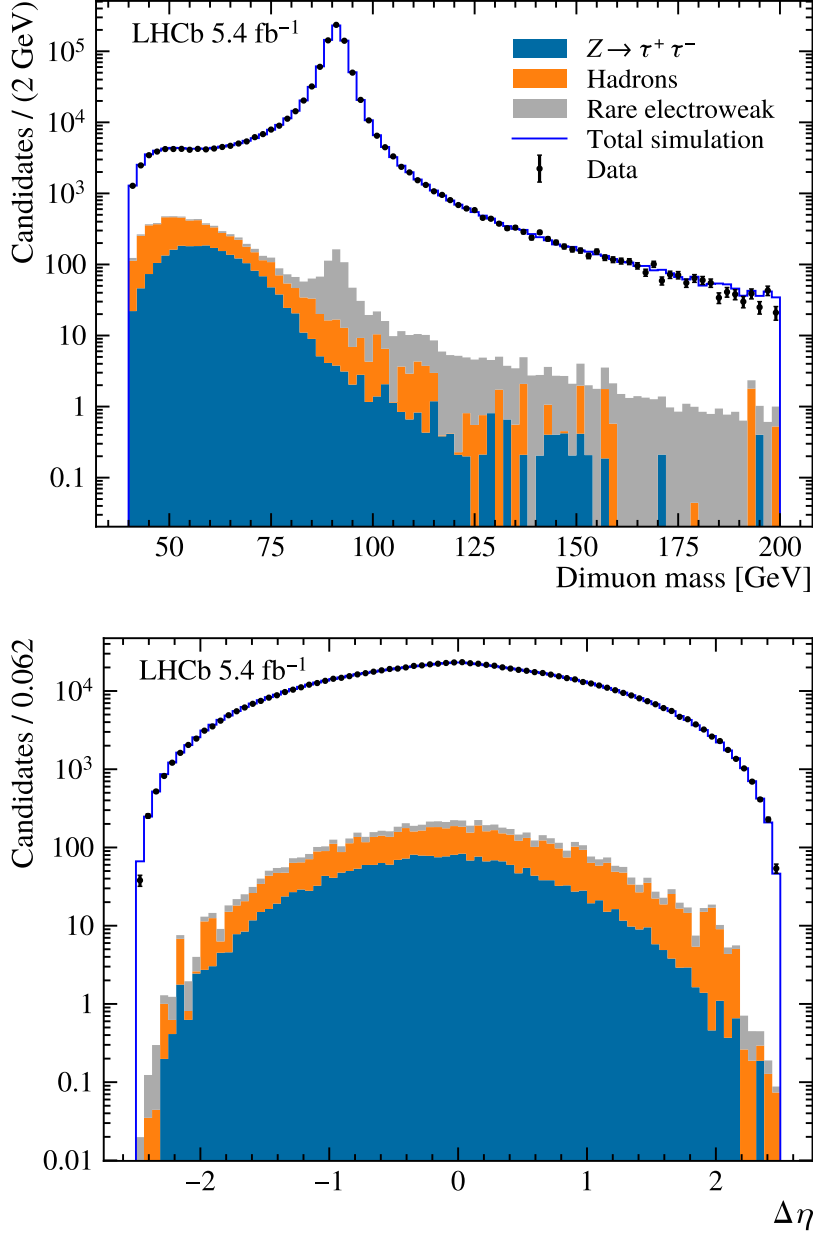


Figure 1: Distributions of (top) dimuon invariant mass and (bottom) $\Delta\eta$ for the selected signal candidates compared to simulation. The dark blue solid line corresponds to the sum of the expected signal and background contributions.

204 4.1 Detector effects

205 The measured value of A_{FB} in each $|\Delta\eta|$ interval is corrected using a term determined
 206 in simulation, $A_{\text{FB}}^{\text{true}} - A_{\text{FB}}^{\text{reco}}$. The value of $A_{\text{FB}}^{\text{true}}$ is defined using truth information and
 207 all events in the fiducial acceptance, while $A_{\text{FB}}^{\text{reco}}$ is defined using reconstruction-level
 208 information and only the events which pass the analysis selection requirements. This
 209 therefore corrects for:

- 210 1. events missed due to detection and selection inefficiencies;

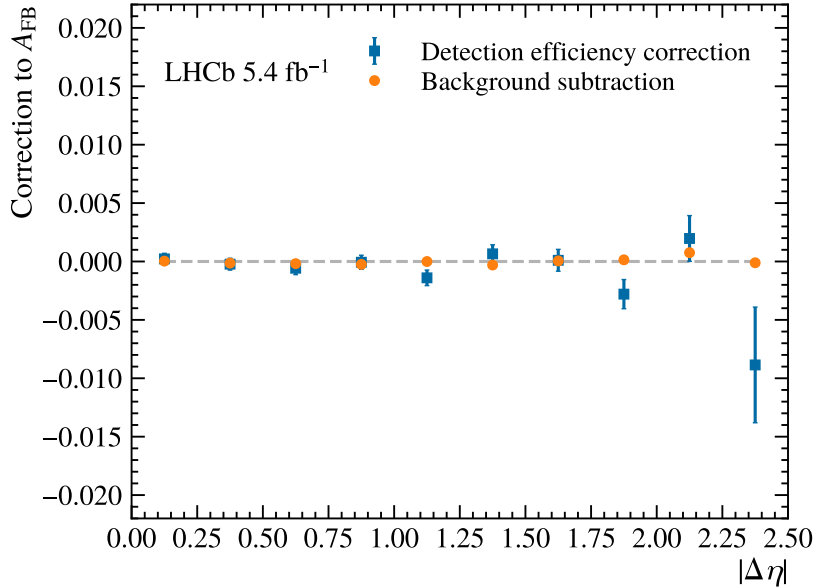


Figure 2: Effects of the detection efficiency correction and background subtraction on the measured A_{FB} in ten intervals of $|\Delta\eta|$, shown in terms of the shift they introduce (ΔA_{FB}). All intervals are defined within the volume $|\Delta\eta| < 2.5$ and $66 < M < 116$ GeV. The error bars on the efficiency correction represent statistical uncertainties only, while the statistical uncertainties on the background subtraction are negligible.

- 211 2. events missed due to (net) migration across boundaries in p_{T} , η and dimuon mass,
 212 and moving in and out of the acceptance;
- 213 3. events reconstructed in the wrong interval of $|\Delta\eta|$.

214 This last effect is negligible since the detector resolution on $|\Delta\eta|$ is excellent. An additional
 215 cross-check is performed incorporating this specific effect as a separate correction, which
 216 finds a negligible change in the final results. The overall correction could depend on the
 217 size of the weak mixing angle assumed in simulation. Both the correction and the final
 218 result are stable with respect to large changes in the assumed value of the weak mixing
 219 angle.

220 4.2 Systematic uncertainties

221 Figure 3 shows the sizes of the systematic uncertainties on A_{FB} in the $|\Delta\eta|$ intervals.
 222 These uncertainties are defined as follows.

223 **Detection efficiency:** The statistical uncertainties on the trigger, muon identification
 224 and tracking efficiency corrections are propagated by randomly varying the estimated
 225 efficiencies within their uncertainties and then redetermining the parameters of the
 226 p_{T} -dependent functions. This is then propagated through the measurement of
 227 A_{FB} . For each efficiency factor, the uncertainty is defined by the root mean square
 228 of the resulting distribution of A_{FB} values after the random variations. Discrete
 229 variations in the efficiency correction method are also considered. Tighter and looser
 230 requirements on the dimuon invariant mass and on the muon selection criteria are

231 considered as an additional source of uncertainty in the determination of the muon
 232 efficiencies. Since the efficiencies are studied in intervals covering detector regions,
 233 the number of intervals is varied. The variation that induces the largest change in
 234 A_{FB} is then used to set an uncertainty. In addition, three alternative functional
 235 forms for the p_{T} -dependence of the efficiency corrections are also considered in
 236 the same way. Each contribution is then combined in quadrature to set an overall
 237 detection efficiency uncertainty.

238 **Backgrounds:** The cross-section assumed for the heavy-flavour-hadron background is
 239 varied up and down by 50% with the resulting shifts in the measured A_{FB} is defined
 240 as the associated uncertainty. The contribution from $Z \rightarrow \tau^+\tau^-$ decays occurs at
 241 a similar rate to the heavy-flavour-hadron background, but is known to far better
 242 precision, and consequently the uncertainty associated with this process is negligible.
 243 No uncertainty is assigned for other, smaller backgrounds.

244 **Physics modelling:** Weights are assigned to the signal events such that the kinematic
 245 distributions match the predictions of the DYTURBO program [31], which has
 246 a higher formal accuracy than PYTHIA 8. The cross-section is predicted using
 247 DYTURBO in intervals of boson p_{T} , mass and rapidity, with logarithms in p_{T}/M
 248 resummed to next-to-next-to-leading order (NNLO), while the angular coefficients
 249 are predicted at NLO in the strong coupling. These weights primarily affect the
 250 A_{FB} measurement via changes in the detection efficiency correction. The shift in
 251 the A_{FB} measurement sets the uncertainty.

252 The statistical uncertainties on the pseudomass calibrations and the momentum smearing
 253 are propagated through the A_{FB} measurement, but their effect is found to be negligible,
 254 which is expected since the measurement only has a single wide interval in mass. The
 255 total uncertainty is found by combining the contributions from these different sources in
 256 quadrature.

257 4.3 Results

258 Table 1 and Fig. 4 report the measured A_{FB} values in the ten intervals of $|\Delta\eta|$. There
 259 are no correlations between the statistical uncertainties. The correlation matrix of the
 260 systematic uncertainties is presented in Table 2.

261 5 Determination of the effective leptonic weak mixing 262 angle

263 In order to determine the value of $\sin^2\theta_{\text{eff}}^\ell$ that best describes the measured A_{FB} distribu-
 264 tion, predictions of A_{FB} are produced using the POWHEG-BOX program [32–34], using
 265 different configurations.

266 The baseline prediction, hereafter referred to as ‘POWHEG-ewnl0’, takes NLO accuracy
 267 for both QCD and electroweak interactions [35, 36], using the scheme described in Ref. [37],
 268 that takes G_μ , m_Z and $\sin^2\theta_{\text{eff}}^\ell$ as inputs. The events produced are then processed with
 269 PHOTOS [38] for modelling of additional QED radiation and with PYTHIA 8 [20] for
 270 simulating the rest of the event.

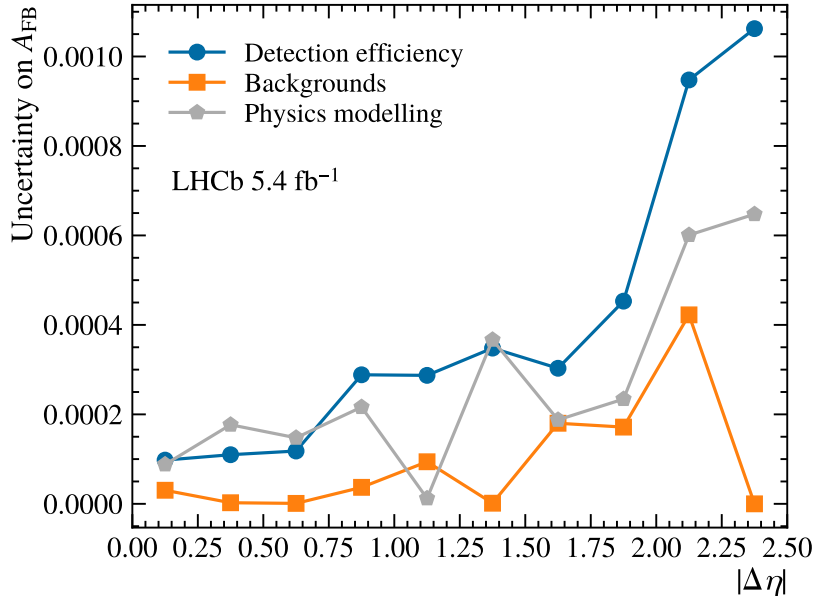


Figure 3: Systematic uncertainties on the A_{FB} measurement in $|\Delta\eta|$ intervals.

Table 1: Results of the A_{FB} measurement. The first uncertainty is statistical and the second is systematic.

Interval number	Interval	A_{FB}
0	$0.00 < \Delta\eta \leq 0.25$	$0.0036 \pm 0.0025 \pm 0.0001$
1	$0.25 < \Delta\eta \leq 0.50$	$0.0204 \pm 0.0027 \pm 0.0002$
2	$0.50 < \Delta\eta \leq 0.75$	$0.0303 \pm 0.0028 \pm 0.0002$
3	$0.75 < \Delta\eta \leq 1.00$	$0.0406 \pm 0.0031 \pm 0.0003$
4	$1.00 < \Delta\eta \leq 1.25$	$0.0466 \pm 0.0034 \pm 0.0002$
5	$1.25 < \Delta\eta \leq 1.50$	$0.0528 \pm 0.0039 \pm 0.0004$
6	$1.50 < \Delta\eta \leq 1.75$	$0.0622 \pm 0.0047 \pm 0.0003$
7	$1.75 < \Delta\eta \leq 2.00$	$0.0545 \pm 0.0060 \pm 0.0004$
8	$2.00 < \Delta\eta \leq 2.25$	$0.0603 \pm 0.0088 \pm 0.0010$
9	$2.25 < \Delta\eta \leq 2.50$	$0.0622 \pm 0.0190 \pm 0.0008$

271 Further predictions are produced to study modelling variations. Events are generated
272 using the configuration described above but with the electroweak interactions simulated at
273 LO accuracy; this is referred to as ‘POWHEG-ewlo’. Predictions are also produced using
274 an alternative calculation of the single-boson process in POWHEG-BOX [39] where QCD
275 interactions are simulated at NLO accuracy and electroweak interactions are simulated at
276 LO accuracy. For this prediction both additional QED radiation and additional simulation
277 of the rest of the event are performed using PYTHIA 8. This configuration is labelled
278 ‘POWHEG-plain’. These predictions are validated by producing an additional set of
279 theoretical predictions using the G_μ input scheme [37] using both POWHEG-BOX and
280 DYTURBO [31]. The two predicted A_{FB} distributions show excellent agreement.

281 The baseline description of the proton internal structure in all predictions uses the
282 parton distributions from the central NNPDF3.1 PDF set at NLO [40]. Event weights

283 are then used to recast the POWHEG-plain predictions to alternative parton distributions
 284 functions [41]. In this analysis predictions at NLO accuracy using the CT18 [42] and
 285 MSHT [43] descriptions of the proton internal structure are also considered and treated
 286 equally to those from NNPDF3.1. These three descriptions all use broadly comparable
 287 global datasets and do not include the LHCb data studied here in their global fits. Other
 288 descriptions of the proton are also considered (NNPDF 4.0 [44], CT18Z [42]).

289 In addition, events are generated using the POWHEG-plain configuration with variations
 290 in the QCD modelling. Events are generated with the factorisation and renormalisation
 291 scales varied by a factor of two around their baseline values in line with the seven-point
 292 variation approach [45], in order to assess the impact of missing higher-order effects
 293 on the theoretical predictions. Events are also generated with two values of the strong
 294 coupling α_s , 0.118 (the baseline) and 0.125. While this is a large variation with respect to
 295 the uncertainty on the world average value, this shift was observed to best describe the
 296 vector-boson p_T distribution in the LHCb measurement of the W -boson mass [29], and is
 297 again considered as a variation that mimics the effects of higher-order contributions in
 298 the predictions.

299 In order to determine the values of the weak mixing angle that best describe the data,
 300 predictions of A_{FB} are made using events generated with different values of the weak
 301 mixing angle. Predictions for A_{FB} at intermediate values are then found by interpolating
 302 between the generated base predictions. As a cross-check, the effect of including additional
 303 base predictions is also studied.

304 The analysis proceeds through a χ^2 comparison of the measured A_{FB} distribution to
 305 the theoretical predictions with different values of $\sin^2 \theta_{\text{eff}}^\ell$, where the minimum of the χ^2
 306 comparison is used to determine the value of $\sin^2 \theta_{\text{eff}}^\ell$, and the width of the χ^2 parabola is
 307 used to determine the uncertainty. Figure 4 shows the measured A_{FB} values compared to
 308 the predictions with two different $\sin^2 \theta_{\text{eff}}^\ell$ values and the baseline-fit result. The best fit
 309 point has a χ^2 of 8.1 for nine degrees of freedom (ndof), and results in

$$\sin^2 \theta_{\text{eff}}^\ell = 0.23148 \pm 0.00044 \pm 0.00005,$$

310 where the first uncertainty is statistical and the second results from propagating the
 311 systematic uncertainties on the A_{FB} measurement.

Table 2: Correlation coefficients for the experimental systematic uncertainties on the A_{FB} measurement in ten intervals of $|\Delta\eta|$, with the interval numbers indicated as defined in Table 1.

	0	1	2	3	4	5	6	7	8	9
0	+1.00	-0.57	-0.66	-0.62	-0.16	-0.66	-0.83	-0.90	+0.31	+0.76
1	-0.57	+1.00	+0.92	+0.63	-0.09	+0.91	+0.45	+0.33	-0.68	-0.50
2	-0.66	+0.92	+1.00	+0.44	+0.22	+0.77	+0.41	+0.37	-0.82	-0.40
3	-0.62	+0.63	+0.44	+1.00	-0.62	+0.86	+0.60	+0.59	-0.15	-0.89
4	-0.16	-0.09	+0.22	-0.62	+1.00	-0.33	+0.08	+0.12	-0.18	+0.47
5	-0.66	+0.91	+0.77	+0.86	-0.33	+1.00	+0.63	+0.52	-0.47	-0.74
6	-0.83	+0.45	+0.41	+0.60	+0.08	+0.63	+1.00	+0.93	+0.11	-0.67
7	-0.90	+0.33	+0.37	+0.59	+0.12	+0.52	+0.93	+1.00	+0.07	-0.70
8	+0.31	-0.68	-0.82	-0.15	-0.18	-0.47	+0.11	+0.07	+1.00	+0.13
9	+0.76	-0.50	-0.40	-0.89	+0.47	-0.74	-0.67	-0.70	+0.13	+1.00

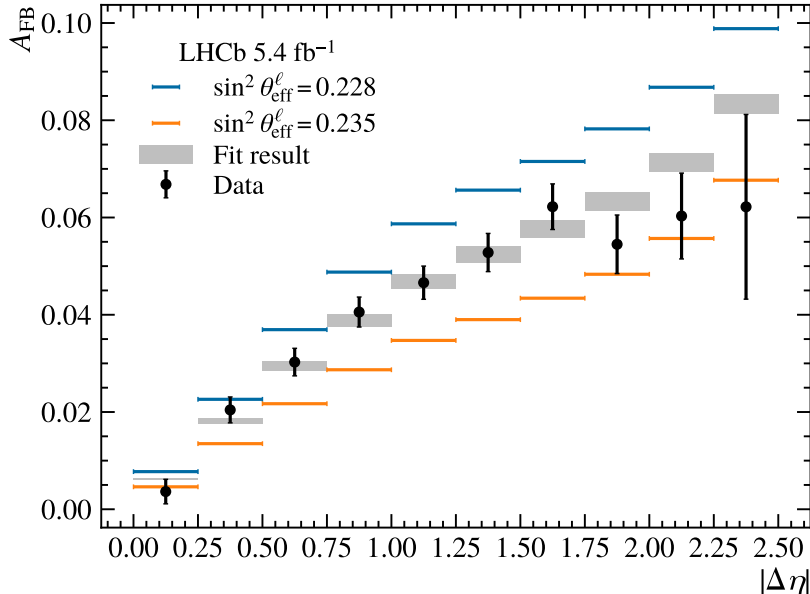


Figure 4: Measured A_{FB} in ten intervals of $|\Delta\eta|$, with the results of the $\sin^2\theta_{\text{eff}}^\ell$ fit. The grey band shows the fit result and the associated statistical uncertainty.

Several variations in the fit model are considered. Some of these variations are used to determine shifts to this result, while others set uncertainties or define cross-checks.

The default analysis uses two base templates for the A_{FB} predictions at different values of $\sin^2\theta_{\text{eff}}^\ell$, with linear interpolation used to find predictions for A_{FB} between these values. However, the impact of using a third base template is studied, applying cubic spline interpolation. A shift to the extracted result corresponding to the difference between these two approaches is applied, so that the final result is based on the cubic approach.³ This provides a shift of $+2.0 \times 10^{-5}$, consistent with the uncertainty associated with the number of generated events used to find the theoretical predictions. The resulting measurement of $\sin^2\theta_{\text{eff}}^\ell$ is then found to be stable at the 1×10^{-5} level when the number of base templates is further increased to seven, confirming that the use of a small number of templates for the baseline result is reasonable.

An electroweak uncertainty of 7.4×10^{-5} is assigned based on the difference between the result found using the POWHEG-ewnl0 and POWHEG-plain predictions. A cross-check is made using the POWHEG-ewlo predictions, which are found to give results in agreement with POWHEG-plain, as expected.

A QCD uncertainty is assigned based on changing the value of α_s used in the POWHEG-plain predictions to the value best describing the data in the LHCb W -boson mass measurement [29]. Since the change in the final result is smaller than the uncertainty on this shift from the number of generated events, the latter is assigned as the uncertainty on $\sin^2\theta_{\text{eff}}^\ell$, 5.8×10^{-5} . The number is consistent with an alternative estimate of the QCD uncertainty using predictions generated with the factorisation and renormalisation scales varied using the seven-point-variation method [45].

The CT18, MSHT20 and NNPDF3.1 PDF parameterisations are treated equally. The

³The application of this shift is equivalent to using three templates to find the central result, but only using two templates to evaluate uncertainties.

Table 3: Fit results, using POWHEG-plain, for different PDF sets. The best-fit $\sin^2 \theta_{\text{eff}}^\ell$ values are listed, as are the PDF uncertainties and the shifts in the $\sin^2 \theta_{\text{eff}}^\ell$ values with respect to the first row. The final row shows the shift that would be applied to the baseline result in order to emulate an arithmetic average of the three PDF sets, and the corresponding PDF uncertainty. The numbers presented in this table do not include the shift associated with changing from two base templates to three base templates. The PDF sets are labeled using the appropriate strings that fully define the set. [46]

PDF set	Value	PDF uncertainty	Shift
NNPDF31_nlo_as0118	0.23155	0.00023	–
CT18NLO	0.23165	0.00022	+0.00010
MSHT20nlo_as118	0.23137	0.00017	–0.00018
Arithmetic average	–	0.00021	–0.00003

336 final result quoted is therefore defined as the arithmetic average of the results from the
337 three parameterisations. The impact of changing the PDF parameterisation is studied
338 using POWHEG-plain events. The PDF uncertainties are determined for each PDF set
339 using the prescription provided by each PDF-fitting group, by weighting the baseline events
340 generated using the central NNPDF3.1 parameterisation. The CT18 uncertainties are
341 divided by a factor 1.645 in order to provide 68% coverage. It is found that changing from
342 the baseline NNPDF3.1 result to the arithmetic average results in a shift of -3×10^{-5} . The
343 PDF parameterisations are treated as fully correlated since they consider the same global
344 data, and therefore the individual PDF uncertainties from the three parameterisations are
345 averaged in order to set the overall PDF uncertainty on the measurement. The results
346 from the different PDF sets are reported in Table 3.

347 The impact of recasting the result to other PDF sets is also studied. The use of the
348 NNPDF4.0 PDF parameterisation leads to the extracted value of $\sin^2 \theta_{\text{eff}}^\ell$ changing by
349 -14×10^{-5} relative to the result found using the NNPDF3.1 parameterisation, while
350 the CT18Z PDF parameterisation changes the result by -8×10^{-5} , again relative to the
351 NNPDF3.1 result.

352 Having applied the relevant shifts and uncertainties defined above which account for:
353 using a larger number of base templates; averaging the three different PDF parameterisa-
354 tions; and the theoretical uncertainties, the final result is

$$\sin^2 \theta_{\text{eff}}^\ell = 0.23147 \pm 0.00044 \pm 0.00005 \pm 0.00023,$$

355 where the first uncertainty is statistical, the second is associated with systematic uncer-
356 tainties on the A_{FB} measurement, and the third is associated with theoretical uncertainties
357 on the model used to determine the weak mixing angle. Figure 5 compares this result with
358 other measurements and with the Standard Model predictions. The LHCb measurement
359 is in excellent agreement with previous measurements and with indirect determinations of
360 the weak mixing angle from the global electroweak fit. It is also notable that while the
361 theoretical uncertainty on the result is dominated by the PDF uncertainty, this uncer-
362 tainty is also significantly smaller than the statistical uncertainty on the measurement.
363 Consequently this analysis does not need to make use of profiling techniques to control
364 and reduce the PDF uncertainty [47, 48].

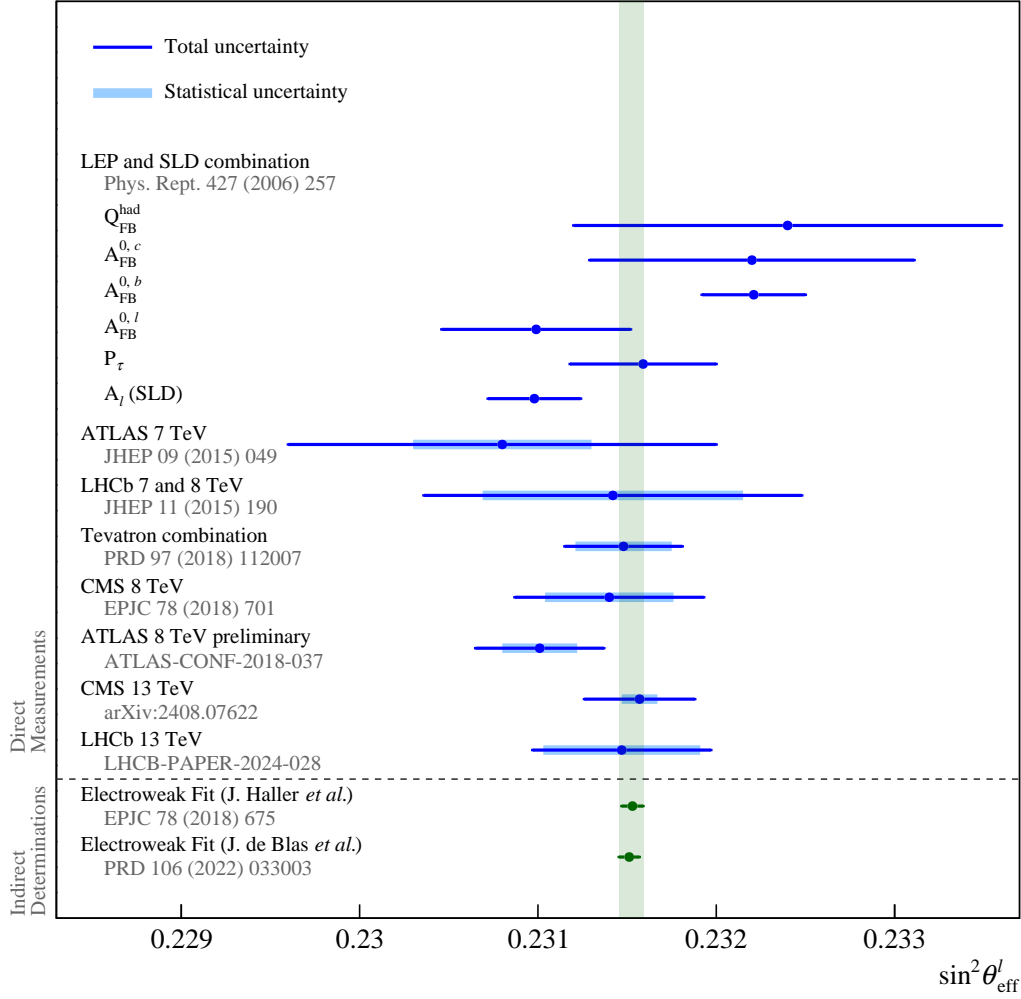


Figure 5: Direct measurements and indirect determinations of $\sin^2 \theta_{\text{eff}}^\ell$. For the measurements from LEP and SLD only the total uncertainty is shown. The indirect determinations shown here include the LEP and SLD measurements as separate inputs while predicting the measurement at hadron colliders.

6 Cross-checks

Various cross-checks are performed to confirm the robustness of the data analysis. In these checks the baseline fit is performed. No shifts are applied to account for the change from two to three base templates, and no average is taken across the different PDF sets. In addition, no systematic uncertainties are considered when performing these checks.

Table 4 shows $\sin^2 \theta_{\text{eff}}^\ell$ fit results with the data divided into statistically independent subsets according to the year of data taking, the polarity of the magnet and the orientation of the decay with respect to the magnetic field, which is characterised by the angle ϕ_d .⁴ All three sets of results are self-consistent within their statistical uncertainties.

⁴See, for example, Eq. 5 of Ref. [28].

Table 4: Fit results with different subsets of the data. For each subset, the first line is treated as the reference for the calculation of the pull. Each row has the same number of intervals and a ndof of 9.

Subset	$\sin^2 \theta_{\text{eff}}^\ell$	Fit χ^2	Pull
2016	0.23014 ± 0.00082	2.0	–
2017	0.23155 ± 0.00085	13.4	+1.2 σ
2018	0.23242 ± 0.00077	10.5	+2.0 σ
Down polarity	0.23087 ± 0.00065	8.2	–
Up polarity	0.23211 ± 0.00065	12.1	1.4 σ
$0 \leq \phi_d < \frac{\pi}{2}$	0.23136 ± 0.00065	10.1	–
$\frac{\pi}{2} \leq \phi_d < \pi$	0.23161 ± 0.00065	6.5	+0.3 σ

Table 5: Fit results with different numbers of $|\Delta\eta|$ intervals. The first row is the reference for the shift, and the uncertainties are statistical only.

Number of intervals	$\sin^2 \theta_{\text{eff}}^\ell$	Shift	Fit χ^2/ndof
1	0.23151 ± 0.00050	–	–
4	0.23167 ± 0.00045	+0.00016	3.1/3
6	0.23145 ± 0.00044	–0.00004	3.2/5
8	0.23146 ± 0.00044	–0.00003	11.7/7
10	0.23148 ± 0.00044	–0.00003	8.1/9

374 Table 5 presents $\sin^2 \theta_{\text{eff}}^\ell$ fit results with different numbers of intervals in $|\Delta\eta|$, varying
375 between one and ten. Compared to the result with a single interval, a relative improvement
376 in the statistical precision of around 14%, as already discussed, is seen in the result with
377 ten intervals. The χ^2 values are reasonable in all cases, and the shifts in the central values
378 are small, considering the statistical uncertainty on the shift between the result with one
379 interval and those with multiple intervals.

380 As an alternative approach, the analysis is performed with a single $|\Delta\eta|$ interval but
381 with seven bins in the dimuon invariant mass. Since the mass is measured with a resolution
382 of $\mathcal{O}(1 \text{ GeV})$, the migration is corrected for using iterative Bayesian unfolding [49]. This
383 leads to a measurement of $\sin^2 \theta_{\text{eff}}^\ell = 0.23130 \pm 0.00050$, with a χ^2/ndof of 14.6/6. The
384 statistical precision of this check is poorer, by 14%, compared to our preferred approach
385 of measuring A_{FB} in intervals of $|\Delta\eta|$. The results remain stable when the number of
386 intervals in the dimuon invariant mass is varied.

387 The following additional checks are also performed:

- 388 • In the A_{FB} measurement, weights are assigned to the simulated signal events that
389 shift the assumed $\sin^2 \theta_{\text{eff}}^\ell$ value. A shift corresponding to three times the uncertainty
390 on the current world average causes a change in our measured $\sin^2 \theta_{\text{eff}}^\ell$ value below
391 2×10^{-5} , which is considered negligible.
- 392 • In addition to the results presented in Table 4, measurements of A_{FB} are performed
393 with six orthogonal combinations of the year and magnet polarity. The resulting
394 $\sin^2 \theta_{\text{eff}}^\ell$ results are statistically consistent.
- 395 • Variations in the $\mathcal{T}(1S)$ and J/ψ masses, within the uncertainties on their world

396 averages, are propagated through the momentum calibrations; the effect on the
397 measured A_{FB} is negligibly small.

- 398 • An alternative functional form is used in the momentum smearing which has a
399 negligible effect on the results quoted.
- 400 • Shifting the muon energies in the simulation, according to the uncertainties in the
401 material budget of the detector, has a negligible effect on the results.

402 7 Conclusion

403 The effective leptonic weak mixing angle, $\sin^2 \theta_{\text{eff}}^\ell$, is precisely predicted in the global
404 electroweak fit. Direct measurements of this predicted quantity are sensitive to physics
405 beyond the Standard Model. A measurement of $\sin^2 \theta_{\text{eff}}^\ell$ is reported, based on pp collision
406 data at $\sqrt{s} = 13$ TeV, recorded between 2016 and 2018 by the LHCb experiment and
407 corresponding to an integrated luminosity of 5.4 fb^{-1} . The forward-backward asymmetry
408 A_{FB} in the $pp \rightarrow Z/\gamma^* \rightarrow \mu^+\mu^-$ process is measured in ten intervals of the difference of
409 the muon pseudorapidities, within a fiducial region covering dimuon masses between 66
410 and 116 GeV, muon pseudorapidities between 2.0 and 4.5 and muon transverse momenta
411 above 20 GeV. Comparing these forward-backward asymmetries with predictions at next-
412 to-leading-order in the strong and electroweak couplings results in a determination of the
413 effective leptonic weak mixing angle

$$\sin^2 \theta_{\text{eff}}^\ell = 0.23147 \pm 0.00044 \pm 0.00005 \pm 0.00023,$$

414 where the first uncertainty is statistical, the second is due to systematic uncertainties on
415 the A_{FB} measurement, and the third is due to theoretical uncertainties associated with
416 the model used to determine the weak mixing angle. This result is based on an arithmetic
417 average of results obtained using the CT18, MSHT20, and NNPDF3.1 parameterisations
418 of the proton internal structure. The result is consistent with other direct measurements
419 and with predictions from the global electroweak fit, and improves on the precision of the
420 previous LHCb determination by more than a factor two.

421 Acknowledgements

422 We express our gratitude to our colleagues in the CERN accelerator departments for the
423 excellent performance of the LHC. We thank the technical and administrative staff at the
424 LHCb institutes. We acknowledge support from CERN and from the national agencies:
425 CAPES, CNPq, FAPERJ and FINEP (Brazil); MOST and NSFC (China); CNRS/IN2P3
426 (France); BMBF, DFG and MPG (Germany); INFN (Italy); NWO (Netherlands); MNiSW
427 and NCN (Poland); MCID/IFA (Romania); MICIU and AEI (Spain); SNSF and SER
428 (Switzerland); NASU (Ukraine); STFC (United Kingdom); DOE NP and NSF (USA). We
429 acknowledge the computing resources that are provided by CERN, IN2P3 (France), KIT
430 and DESY (Germany), INFN (Italy), SURF (Netherlands), PIC (Spain), GridPP (United
431 Kingdom), CSCS (Switzerland), IFIN-HH (Romania), CBPF (Brazil), and Polish WLCG
432 (Poland). We are indebted to the communities behind the multiple open-source software
433 packages on which we depend. Individual groups or members have received support from

434 ARC and ARDC (Australia); Key Research Program of Frontier Sciences of CAS, CAS
435 PIFI, CAS CCEPP, Fundamental Research Funds for the Central Universities, and Sci.
436 & Tech. Program of Guangzhou (China); Minciencias (Colombia); EPLANET, Marie
437 Skłodowska-Curie Actions, ERC and NextGenerationEU (European Union); A*MIDEX,
438 ANR, IPhU and Labex P2IO, and Région Auvergne-Rhône-Alpes (France); AvH Founda-
439 tion (Germany); ICSC (Italy); Severo Ochoa and María de Maeztu Units of Excellence,
440 GVA, XuntaGal, GENCAT, InTalent-Inditex and Prog. Atracción Talento CM (Spain);
441 SRC (Sweden); the Leverhulme Trust, the Royal Society and UKRI (United Kingdom).

442 References

- 443 [1] ALEPH, DELPHI, L3, OPAL, SLD, LEP Electroweak Working Group, SLD Elec-
444 troweak Group, SLD Heavy Flavour Group, S. Schael *et al.*, *Precision electroweak mea-*
445 *surements on the Z resonance*, *Phys. Rept.* **427** (2006) 257, [arXiv:hep-ex/0509008](#).
- 446 [2] J. Haller *et al.*, *Update of the global electroweak fit and constraints on two-Higgs-*
447 *doublet models*, *Eur. Phys. J.* **C78** (2018) 675, [arXiv:1803.01853](#).
- 448 [3] J. de Blas *et al.*, *Global analysis of electroweak data in the standard model*, *Phys. Rev.*
449 **D106** (2022) 033003, [arXiv:2112.07274](#).
- 450 [4] SLD collaboration, K. Abe *et al.*, *An improved direct measurement of leptonic*
451 *coupling asymmetries with polarized Z bosons*, *Phys. Rev. Lett.* **86** (2001) 1162,
452 [arXiv:hep-ex/0010015](#).
- 453 [5] ATLAS collaboration, *Measurement of the effective leptonic weak mixing angle using*
454 *electron and muon pairs from Z-boson decay in the ATLAS experiment at $\sqrt{s} = 8$*
455 *TeV*, ATLAS-CONF-2018-037 (2018).
- 456 [6] CMS collaboration, A. Hayrapetyan *et al.*, *Measurement of the Drell–Yan forward-*
457 *backward asymmetry and of the effective leptonic weak mixing angle in proton-proton*
458 *collisions at $\sqrt{s} = 13$ TeV*, [arXiv:2408.07622](#).
- 459 [7] LHCb collaboration, R. Aaij *et al.*, *Measurement of the forward-backward asymmetry*
460 *in $Z/\gamma^* \rightarrow \mu^+\mu^-$ decays and determination of the effective weak mixing angle*, *JHEP*
461 **11** (2015) 190, [arXiv:1509.07645](#).
- 462 [8] CDF, D0 collaboration, T. A. Aaltonen *et al.*, *Tevatron Run II combination of*
463 *the effective leptonic electroweak mixing angle*, *Phys. Rev.* **D97** (2018) 112007,
464 [arXiv:1801.06283](#).
- 465 [9] J. C. Collins and D. E. Soper, *Angular distribution of dileptons in high-energy hadron*
466 *collisions*, *Phys. Rev.* **D16** (1977) 2219.
- 467 [10] J. G. Korner and E. Mirkes, *Polarization density matrix of high q_T gauge bosons in*
468 *high-energy proton-antiproton collisions*, *Nucl. Phys. B Proc. Suppl.* **23** (1991) 9.
- 469 [11] A. Bodek, *A simple event weighting technique for optimizing the measurement of the*
470 *forward-backward asymmetry of Drell–Yan dilepton pairs at hadron colliders*, *Eur.*
471 *Phys. J.* **C67** (2010) 321, [arXiv:0911.2850](#).

- 472 [12] A. Banfi *et al.*, *Optimisation of variables for studying dilepton transverse momentum*
473 *distributions at hadron colliders*, *Eur. Phys. J.* **C71** (2011) 1600, [arXiv:1009.1580](#).
- 474 [13] LHCb collaboration, A. A. Alves Jr. *et al.*, *The LHCb detector at the LHC*, *JINST* **3**
475 (2008) S08005.
- 476 [14] LHCb collaboration, R. Aaij *et al.*, *LHCb detector performance*, *Int. J. Mod. Phys.*
477 **A30** (2015) 1530022, [arXiv:1412.6352](#).
- 478 [15] R. Aaij *et al.*, *Performance of the LHCb Vertex Locator*, *JINST* **9** (2014) P09007,
479 [arXiv:1405.7808](#).
- 480 [16] P. d'Argent *et al.*, *Improved performance of the LHCb Outer Tracker in LHC Run 2*,
481 *JINST* **12** (2017) P11016, [arXiv:1708.00819](#).
- 482 [17] M. Adinolfi *et al.*, *Performance of the LHCb RICH detector at the LHC*, *Eur. Phys.*
483 *J.* **C73** (2013) 2431, [arXiv:1211.6759](#).
- 484 [18] A. A. Alves Jr. *et al.*, *Performance of the LHCb muon system*, *JINST* **8** (2013)
485 P02022, [arXiv:1211.1346](#).
- 486 [19] R. Aaij *et al.*, *Design and performance of the LHCb trigger and full real-time recon-*
487 *struction in Run 2 of the LHC*, *JINST* **14** (2019) P04013, [arXiv:1812.10790](#).
- 488 [20] T. Sjöstrand, S. Mrenna, and P. Skands, *A brief introduction to PYTHIA*
489 *8.1*, *Comput. Phys. Commun.* **178** (2008) 852, [arXiv:0710.3820](#); T. Sjöstrand,
490 S. Mrenna, and P. Skands, *PYTHIA 6.4 physics and manual*, *JHEP* **05** (2006) 026,
491 [arXiv:hep-ph/0603175](#).
- 492 [21] I. Belyaev *et al.*, *Handling of the generation of primary events in Gauss, the LHCb*
493 *simulation framework*, *J. Phys. Conf. Ser.* **331** (2011) 032047.
- 494 [22] D. J. Lange, *The EvtGen particle decay simulation package*, *Nucl. Instrum. Meth.*
495 **A462** (2001) 152.
- 496 [23] N. Davidson, T. Przedzinski, and Z. Was, *PHOTOS interface in C++: Technical*
497 *and physics documentation*, *Comp. Phys. Comm.* **199** (2016) 86, [arXiv:1011.0937](#).
- 498 [24] Geant4 collaboration, J. Allison *et al.*, *Geant4 developments and applications*, *IEEE*
499 *Trans. Nucl. Sci.* **53** (2006) 270; Geant4 collaboration, S. Agostinelli *et al.*, *Geant4:*
500 *A simulation toolkit*, *Nucl. Instrum. Meth.* **A506** (2003) 250.
- 501 [25] M. Clemencic *et al.*, *The LHCb simulation application, Gauss: Design, evolution and*
502 *experience*, *J. Phys. Conf. Ser.* **331** (2011) 032023.
- 503 [26] LHCb collaboration, R. Aaij *et al.*, *Momentum scale calibration of the LHCb spec-*
504 *trometer*, *JINST* **19** (2024) P02008, [arXiv:2312.01772](#).
- 505 [27] W. Barter, M. Pili, and M. Vesterinen, *A simple method to determine curvature biases*
506 *in track reconstruction in hadron collider experiments*, *Eur. Phys. J.* **C81** (2021) 251,
507 [arXiv:2101.05675](#).

- 508 [28] LHCb collaboration, R. Aaij *et al.*, *Charge-dependent curvature-bias corrections using*
509 *a pseudomass method*, *JINST* **19** (2024) P03010, [arXiv:2311.04670](#).
- 510 [29] LHCb collaboration, R. Aaij *et al.*, *Measurement of the W boson mass*, *JHEP* **01**
511 (2022) 036, [arXiv:2109.01113](#).
- 512 [30] LHCb collaboration, R. Aaij *et al.*, *Measurement of the track reconstruction efficiency*
513 *at LHCb*, *JINST* **10** (2015) P02007, [arXiv:1408.1251](#).
- 514 [31] S. Camarda *et al.*, *DYTurbo: fast predictions for Drell–Yan processes*, *Eur. Phys. J.*
515 **C80** (2020) 251, Erratum *ibid.* **C80** (2020) 440, [arXiv:1910.07049](#).
- 516 [32] P. Nason, *A New method for combining NLO QCD with shower Monte Carlo algo-*
517 *rithms*, *JHEP* **11** (2004) 040, [arXiv:hep-ph/0409146](#).
- 518 [33] S. Frixione, P. Nason, and C. Oleari, *Matching NLO QCD computations with parton*
519 *shower simulations: the POWHEG method*, *JHEP* **11** (2007) 070, [arXiv:0709.2092](#).
- 520 [34] S. Alioli, P. Nason, C. Oleari, and E. Re, *A general framework for implementing*
521 *NLO calculations in shower Monte Carlo programs: the POWHEG BOX*, *JHEP* **06**
522 (2010) 043, [arXiv:1002.2581](#).
- 523 [35] L. Barze *et al.*, *Neutral current Drell–Yan with combined QCD and electroweak*
524 *corrections in the POWHEG BOX*, *Eur. Phys. J.* **C73** (2013) 2474, [arXiv:1302.4606](#).
- 525 [36] M. Chiesa, C. L. Del Pio, and F. Piccinini, *On electroweak corrections to neu-*
526 *tral current Drell–Yan with the POWHEG BOX*, *Eur. Phys. J.* **C84** (2024) 539,
527 [arXiv:2402.14659](#).
- 528 [37] M. Chiesa, F. Piccinini, and A. Vicini, *Direct determination of $\sin^2 \theta_{\text{eff}}^\ell$ at hadron*
529 *colliders*, *Phys. Rev.* **D100** (2019) 071302, [arXiv:1906.11569](#).
- 530 [38] E. Barberio, B. van Eijk, and Z. Was, *PHOTOS: A Universal Monte Carlo for QED*
531 *radiative corrections in decays*, *Comput. Phys. Commun.* **66** (1991) 115.
- 532 [39] S. Alioli, P. Nason, C. Oleari, and E. Re, *NLO vector-boson production matched with*
533 *shower in POWHEG*, *JHEP* **07** (2008) 060, [arXiv:0805.4802](#).
- 534 [40] NNPDF collaboration, R. D. Ball *et al.*, *Parton distributions from high-precision*
535 *collider data*, *Eur. Phys. J.* **C77** (2017) 663, [arXiv:1706.00428](#).
- 536 [41] A. Buckley *et al.*, *LHAPDF6: parton density access in the LHC precision era*, *Eur.*
537 *Phys. J.* **C75** (2015) 132, [arXiv:1412.7420](#).
- 538 [42] T.-J. Hou *et al.*, *New CTEQ global analysis of quantum chromodynamics with high-*
539 *precision data from the LHC*, *Phys. Rev.* **D103** (2021) 014013, [arXiv:1912.10053](#).
- 540 [43] S. Bailey *et al.*, *Parton distributions from LHC, HERA, Tevatron and fixed target*
541 *data: MSHT20 PDFs*, *Eur. Phys. J.* **C81** (2021) 341, [arXiv:2012.04684](#).
- 542 [44] NNPDF collaboration, R. D. Ball *et al.*, *The path to proton structure at 1% accuracy*,
543 *Eur. Phys. J.* **C82** (2022) 428, [arXiv:2109.02653](#).

- 544 [45] K. Hamilton, P. Nason, E. Re, and G. Zanderighi, *NNLOPS simulation of Higgs*
545 *boson production*, *JHEP* **10** (2013) 222, [arXiv:1309.0017](#).
- 546 [46] A. Buckley *et al.*, *LHAPDF6: parton density access in the LHC precision era*, *Eur.*
547 *Phys. J.* **C75** (2015) 132, [arXiv:1412.7420](#).
- 548 [47] A. Bodek, J. Han, A. Khukhunaishvili, and W. Sakumoto, *Using Drell–Yan for-*
549 *ward–backward asymmetry to reduce PDF uncertainties in the measurement of elec-*
550 *troweak parameters*, *Eur. Phys. J.* **C76** (2016) 115, [arXiv:1507.02470](#).
- 551 [48] P. Azzi *et al.*, *Report from Working Group 1: Standard Model Physics at the HL-LHC*
552 *and HE-LHC*, *CERN Yellow Rep. Monogr.* **7** (2019) 1, [arXiv:1902.04070](#).
- 553 [49] G. D’Agostini, *Improved iterative Bayesian unfolding*, in *Alliance Workshop on*
554 *Unfolding and Data Correction*, 2010, [arXiv:1010.0632](#).

LHCb collaboration

555 R. Aaij³⁷ , A.S.W. Abdelmotteleb⁵⁶ , C. Abellan Beteta⁵⁰ , F. Abudinén⁵⁶ ,
 556 T. Ackernley⁶⁰ , A. A. Adefisoye⁶⁸ , B. Adeva⁴⁶ , M. Adinolfi⁵⁴ , P. Adlarson⁸¹ ,
 557 C. Agapopoulou¹⁴ , C.A. Aidala⁸² , Z. Ajaltouni¹¹ , S. Akar⁶⁵ , K. Akiba³⁷ ,
 558 P. Albicocco²⁷ , J. Albrecht¹⁹ , F. Alessio⁴⁸ , M. Alexander⁵⁹ , Z. Aliouche⁶² ,
 559 P. Alvarez Cartelle⁵⁵ , R. Amalric¹⁶ , S. Amato³ , J.L. Amey⁵⁴ , Y. Amhis^{14,48} ,
 560 L. An⁶ , L. Anderlini²⁶ , M. Andersson⁵⁰ , A. Andreianov⁴³ , P. Andreola⁵⁰ ,
 561 M. Andreotti²⁵ , D. Andreou⁶⁸ , A. Anelli^{30,n} , D. Ao⁷ , F. Archilli^{36,t} ,
 562 M. Argenton²⁵ , S. Arguedas Cuendis^{9,48} , A. Artamonov⁴³ , M. Artuso⁶⁸ ,
 563 E. Aslanides¹³ , R. Ataíde Da Silva⁴⁹ , M. Atzeni⁶⁴ , B. Audurier¹² , D. Bacher⁶³ ,
 564 I. Bachiller Perea¹⁰ , S. Bachmann²¹ , M. Bachmayer⁴⁹ , J.J. Back⁵⁶ ,
 565 P. Baladron Rodriguez⁴⁶ , V. Balagura¹⁵ , W. Baldini²⁵ , L. Balzani¹⁹ , H. Bao⁷ ,
 566 J. Baptista de Souza Leite⁶⁰ , C. Barbero Pretel^{46,12} , M. Barbetti²⁶ , I. R. Barbosa⁶⁹ ,
 567 R.J. Barlow⁶² , M. Barnyakov²⁴ , S. Barsuk¹⁴ , W. Barter⁵⁸ , M. Bartolini⁵⁵ ,
 568 J. Bartz⁶⁸ , J.M. Basels¹⁷ , S. Bashir³⁹ , G. Bassi^{34,q} , B. Batsukh⁵ , P. B. Battista¹⁴ ,
 569 A. Bay⁴⁹ , A. Beck⁵⁶ , M. Becker¹⁹ , F. Bedeschi³⁴ , I.B. Bediaga² , N. A.
 570 Behling¹⁹ , S. Belin⁴⁶ , V. Bellee⁵⁰ , K. Belous⁴³ , I. Belov²⁸ , I. Belyaev³⁵ ,
 571 G. Benane¹³ , G. Bencivenni²⁷ , E. Ben-Haim¹⁶ , A. Berezhnoy⁴³ , R. Bernet⁵⁰ ,
 572 S. Bernet Andres⁴⁴ , A. Bertolin³² , C. Betancourt⁵⁰ , F. Betti⁵⁸ , J. Bex⁵⁵ ,
 573 Ia. Bezshyiko⁵⁰ , J. Bhom⁴⁰ , M.S. Bieker¹⁹ , N.V. Biesuz²⁵ , P. Billoir¹⁶ ,
 574 A. Biolchini³⁷ , M. Birch⁶¹ , F.C.R. Bishop¹⁰ , A. Bitadze⁶² , A. Bizzeti , T. Blake⁵⁶ ,
 575 F. Blanc⁴⁹ , J.E. Blank¹⁹ , S. Blusk⁶⁸ , V. Bocharnikov⁴³ , J.A. Boelhaue¹⁹ ,
 576 O. Boente Garcia¹⁵ , T. Boettcher⁶⁵ , A. Bohare⁵⁸ , A. Boldyrev⁴³ , C.S. Bolognani⁷⁸ ,
 577 R. Bolzonella^{25,k} , N. Bondar⁴³ , A. Bordelius⁴⁸ , F. Borgato^{32,o} , S. Borghi⁶² ,
 578 M. Borsato^{30,n} , J.T. Borsuk⁴⁰ , S.A. Bouchiba⁴⁹ , M. Bovill⁶³ , T.J.V. Bowcock⁶⁰ ,
 579 A. Boyer⁴⁸ , C. Bozzi²⁵ , A. Brea Rodriguez⁴⁹ , N. Breer¹⁹ , J. Brodzicka⁴⁰ ,
 580 A. Brossa Gonzalo^{46,56,45,†} , J. Brown⁶⁰ , D. Brundu³¹ , E. Buchanan⁵⁸ , A. Buonauro⁵⁰ ,
 581 L. Buonincontri^{32,o} , A.T. Burke⁶² , C. Burr⁴⁸ , J.S. Butter⁵⁵ , J. Buytaert⁴⁸ ,
 582 W. Byczynski⁴⁸ , S. Cadeddu³¹ , H. Cai⁷³ , A. C. Caillet¹⁶ , R. Calabrese^{25,k} ,
 583 S. Calderon Ramirez⁹ , L. Calefice⁴⁵ , S. Cali²⁷ , M. Calvi^{30,n} , M. Calvo Gomez⁴⁴ ,
 584 P. Camargo Magalhaes^{2,x} , J. I. Cambon Bouzas⁴⁶ , P. Campana²⁷ ,
 585 D.H. Campora Perez⁷⁸ , A.F. Campoverde Quezada⁷ , S. Capelli³⁰ , L. Capriotti²⁵ ,
 586 R. Caravaca-Mora⁹ , A. Carbone^{24,i} , L. Carcedo Salgado⁴⁶ , R. Cardinale^{28,l} ,
 587 A. Cardini³¹ , P. Carniti^{30,n} , L. Carus²¹ , A. Casais Vidal⁶⁴ , R. Caspary²¹ ,
 588 G. Casse⁶⁰ , J. Castro Godinez⁹ , M. Cattaneo⁴⁸ , G. Cavallero^{25,48} , V. Cavallini^{25,k} ,
 589 S. Celani²¹ , D. Cervenkov⁶³ , S. Cesare^{29,m} , A.J. Chadwick⁶⁰ , I. Chahrour⁸² ,
 590 M. Charles¹⁶ , Ph. Charpentier⁴⁸ , E. Chatzianagnostou³⁷ , M. Chefdeville¹⁰ ,
 591 C. Chen¹³ , S. Chen⁵ , Z. Chen⁷ , A. Chernov⁴⁰ , S. Chernyshenko⁵² , X.
 592 Chiotopoulos⁷⁸ , V. Chobanova⁸⁰ , S. Cholak⁴⁹ , M. Chrzaszcz⁴⁰ , A. Chubykin⁴³ ,
 593 V. Chulikov⁴³ , P. Ciambone²⁷ , X. Cid Vidal⁴⁶ , G. Ciezarek⁴⁸ , P. Cifra⁴⁸ ,
 594 P.E.L. Clarke⁵⁸ , M. Clemencic⁴⁸ , H.V. Cliff⁵⁵ , J. Closier⁴⁸ , C. Cocha Toapaxi²¹ ,
 595 V. Coco⁴⁸ , J. Cogan¹³ , E. Cogneras¹¹ , L. Cojocariu⁴² , P. Collins⁴⁸ ,
 596 T. Colombo⁴⁸ , M. C. Colonna¹⁹ , A. Comerma-Montells⁴⁵ , L. Congedo²³ ,
 597 A. Contu³¹ , N. Cooke⁵⁹ , I. Corredoira⁴⁶ , A. Correia¹⁶ , G. Corti⁴⁸ ,
 598 J.J. Cottee Meldrum⁵⁴ , B. Couturier⁴⁸ , D.C. Craik⁵⁰ , M. Cruz Torres^{2,f} ,
 599 E. Curras Rivera⁴⁹ , R. Currie⁵⁸ , C.L. Da Silva⁶⁷ , S. Dadabaev⁴³ , L. Dai⁷⁰ ,
 600 X. Dai⁶ , E. Dall’Occo¹⁹ , J. Dalseno⁴⁶ , C. D’Ambrosio⁴⁸ , J. Daniel¹¹ ,
 601 A. Danilina⁴³ , P. d’Argent²³ , A. Davidson⁵⁶ , J.E. Davies⁶² , A. Davis⁶² ,
 602 O. De Aguiar Francisco⁶² , C. De Angelis^{31,j} , F. De Benedetti⁴⁸ , J. de Boer³⁷ ,

603 K. De Bruyn⁷⁷ , S. De Capua⁶² , M. De Cian^{21,48} , U. De Freitas Carneiro Da Graca^{2,a} ,
 604 E. De Lucia²⁷ , J.M. De Miranda² , L. De Paula³ , M. De Serio^{23,g} , P. De Simone²⁷ ,
 605 F. De Vellis¹⁹ , J.A. de Vries⁷⁸ , F. Debernardis²³ , D. Decamp¹⁰ , V. Dedu¹³ , S.
 606 Dekkers¹ , L. Del Buono¹⁶ , B. Delaney⁶⁴ , H.-P. Dembinski¹⁹ , J. Deng⁸ ,
 607 V. Denysenko⁵⁰ , O. Deschamps¹¹ , F. Dettori^{31,j} , B. Dey⁷⁶ , P. Di Nezza²⁷ ,
 608 I. Diachkov⁴³ , S. Didenko⁴³ , S. Ding⁶⁸ , L. Dittmann²¹ , V. Dobishuk⁵² , A. D.
 609 Docheva⁵⁹ , C. Dong^{4,b} , A.M. Donohoe²² , F. Dordei³¹ , A.C. dos Reis² , A. D.
 610 Dowling⁶⁸ , W. Duan⁷¹ , P. Duda⁷⁹ , M.W. Dudek⁴⁰ , L. Dufour⁴⁸ , V. Duk³³ ,
 611 P. Durante⁴⁸ , M. M. Duras⁷⁹ , J.M. Durham⁶⁷ , O. D. Durmus⁷⁶ , A. Dziurda⁴⁰ ,
 612 A. Dzyuba⁴³ , S. Easo⁵⁷ , E. Eckstein¹⁸ , U. Egede¹ , A. Egorychev⁴³ ,
 613 V. Egorychev⁴³ , S. Eisenhardt⁵⁸ , E. Ejopu⁶² , L. Eklund⁸¹ , M. Elashri⁶⁵ ,
 614 J. Ellbracht¹⁹ , S. Ely⁶¹ , A. Ene⁴² , E. Epple⁶⁵ , J. Eschle⁶⁸ , S. Esen²¹ ,
 615 T. Evans⁶² , F. Fabiano^{31,j} , L.N. Falcao² , Y. Fan⁷ , B. Fang⁷³ , L. Fantini^{33,p,48} ,
 616 M. Faria⁴⁹ , K. Farmer⁵⁸ , S. Farry⁶⁰ , D. Fazzini^{30,n} , L. Felkowski⁷⁹ , M. Feng^{5,7} ,
 617 M. Feo^{19,48} , A. Fernandez Casani⁴⁷ , M. Fernandez Gomez⁴⁶ , A.D. Fernez⁶⁶ ,
 618 F. Ferrari²⁴ , F. Ferreira Rodrigues³ , M. Ferrillo⁵⁰ , M. Ferro-Luzzi⁴⁸ , S. Filippov⁴³ ,
 619 R.A. Fini²³ , M. Fiorini^{25,k} , M. Firlej³⁹ , K.L. Fischer⁶³ , D.S. Fitzgerald⁸² ,
 620 C. Fitzpatrick⁶² , T. Fiutowski³⁹ , F. Fleuret¹⁵ , M. Fontana²⁴ , L. F. Foreman⁶² ,
 621 R. Forty⁴⁸ , D. Foulds-Holt⁵⁵ , V. Franco Lima³ , M. Franco Sevilla⁶⁶ , M. Frank⁴⁸ ,
 622 E. Franzoso^{25,k} , G. Frau⁶² , C. Frei⁴⁸ , D.A. Friday⁶² , J. Fu⁷ , Q. Fuehring^{19,55} ,
 623 Y. Fujii¹ , T. Fulghesu¹⁶ , E. Gabriel³⁷ , G. Galati²³ , M.D. Galati³⁷ ,
 624 A. Gallas Torreira⁴⁶ , D. Galli^{24,i} , S. Gambetta⁵⁸ , M. Gandelman³ , P. Gandini²⁹ , B.
 625 Ganie⁶² , H. Gao⁷ , R. Gao⁶³ , T.Q. Gao⁵⁵ , Y. Gao⁸ , Y. Gao⁶ , Y. Gao⁸,
 626 M. Garau^{31,j} , L.M. Garcia Martin⁴⁹ , P. Garcia Moreno⁴⁵ , J. García Pardiñas⁴⁸ , K. G.
 627 Garg⁸ , L. Garrido⁴⁵ , C. Gaspar⁴⁸ , R.E. Geertsema³⁷ , L.L. Gerken¹⁹ ,
 628 E. Gersabeck⁶² , M. Gersabeck⁶² , T. Gershon⁵⁶ , S. G. Ghizzo^{28,l},
 629 Z. Ghorbanimoghaddam⁵⁴, L. Giambastiani^{32,o} , F. I. Giasemis^{16,e} , V. Gibson⁵⁵ ,
 630 H.K. Giemza⁴¹ , A.L. Gilman⁶³ , M. Giovannetti²⁷ , A. Gioventù⁴⁵ , L. Girardey⁶² ,
 631 P. Gironella Gironell⁴⁵ , C. Giugliano^{25,k} , M.A. Giza⁴⁰ , E.L. Gkougkousis⁶¹ ,
 632 F.C. Glaser^{14,21} , V.V. Gligorov^{16,48} , C. Göbel⁶⁹ , E. Golobardes⁴⁴ , D. Golubkov⁴³ ,
 633 A. Golutvin^{61,43,48} , S. Gomez Fernandez⁴⁵ , F. Goncalves Abrantes⁶³ , M. Goncerz⁴⁰ ,
 634 G. Gong^{4,b} , J. A. Gooding¹⁹ , I.V. Gorelov⁴³ , C. Gotti³⁰ , J.P. Grabowski¹⁸ ,
 635 L.A. Granada Cardoso⁴⁸ , E. Graugés⁴⁵ , E. Graverini^{49,r} , L. Gazette⁵⁶ ,
 636 G. Graziani , A. T. Grecu⁴² , L.M. Greeven³⁷ , N.A. Grieser⁶⁵ , L. Grillo⁵⁹ ,
 637 S. Gromov⁴³ , C. Gu¹⁵ , M. Guarise²⁵ , L. Guerry¹¹ , M. Guittiere¹⁴ ,
 638 V. Guliaeva⁴³ , P. A. Günther²¹ , A.-K. Guseinov⁴⁹ , E. Gushchin⁴³ , Y. Guz^{6,43,48} ,
 639 T. Gys⁴⁸ , K. Habermann¹⁸ , T. Hadavizadeh¹ , C. Hadjivasiliou⁶⁶ , G. Haefeli⁴⁹ ,
 640 C. Haen⁴⁸ , J. Haimberger⁴⁸ , M. Hajheidari⁴⁸, G. Hallett⁵⁶ , M.M. Halvorsen⁴⁸ ,
 641 P.M. Hamilton⁶⁶ , J. Hammerich⁶⁰ , Q. Han⁸ , X. Han²¹ , S. Hansmann-Menzemer²¹ ,
 642 L. Hao⁷ , N. Harnew⁶³ , M. Hartmann¹⁴ , S. Hashmi³⁹ , J. He^{7,c} , F. Hemmer⁴⁸ ,
 643 C. Henderson⁶⁵ , R.D.L. Henderson^{1,56} , A.M. Hennequin⁴⁸ , K. Hennessy⁶⁰ ,
 644 L. Henry⁴⁹ , J. Herd⁶¹ , P. Herrero Gascon²¹ , J. Heuel¹⁷ , A. Hicheur³ ,
 645 G. Hijano Mendizabal⁵⁰, D. Hill⁴⁹ , S.E. Hollitt¹⁹ , J. Horswill⁶² , R. Hou⁸ , Y. Hou¹¹ ,
 646 N. Howarth⁶⁰, J. Hu²¹, J. Hu⁷¹ , W. Hu⁶ , X. Hu^{4,b} , W. Huang⁷ , W. Hulsbergen³⁷ ,
 647 R.J. Hunter⁵⁶ , M. Hushchyn⁴³ , D. Hutchcroft⁶⁰ , M. Idzik³⁹ , D. Ilin⁴³ , P. Ilten⁶⁵ ,
 648 A. Inglessi⁴³ , A. Injukhin⁴³ , A. Ishteev⁴³ , K. Ivshin⁴³ , R. Jacobsson⁴⁸ , H. Jage¹⁷ ,
 649 S.J. Jaimes Elles^{47,74} , S. Jakobsen⁴⁸ , E. Jans³⁷ , B.K. Jashal⁴⁷ , A. Jawahery^{66,48} ,
 650 V. Jevtic¹⁹ , E. Jiang⁶⁶ , X. Jiang^{5,7} , Y. Jiang⁷ , Y. J. Jiang⁶ , M. John⁶³ , A.
 651 John Rubesh Rajan²² , D. Johnson⁵³ , C.R. Jones⁵⁵ , T.P. Jones⁵⁶ , S. Joshi⁴¹ ,
 652 B. Jost⁴⁸ , J. Juan Castella⁵⁵ , N. Jurik⁴⁸ , I. Juszczak⁴⁰ , D. Kaminaris⁴⁹ ,

653 S. Kandybei⁵¹ , M. Kane⁵⁸ , Y. Kang^{4,b} , C. Kar¹¹ , M. Karacson⁴⁸ ,
654 D. Karpenkov⁴³ , A. Kauniskangas⁴⁹ , J.W. Kautz⁶⁵ , M.K. Kazanecki⁴⁰, F. Keizer⁴⁸ ,
655 M. Kenzie⁵⁵ , T. Ketel³⁷ , B. Khanji⁶⁸ , A. Kharisova⁴³ , S. Kholodenko^{34,48} ,
656 G. Khreich¹⁴ , T. Kirn¹⁷ , V.S. Kirsebom^{30,n} , O. Kitouni⁶⁴ , S. Klaver³⁸ ,
657 N. Kleijne^{34,q} , K. Klimaszewski⁴¹ , M.R. Kmiec⁴¹ , S. Koliiev⁵² , L. Kolk¹⁹ ,
658 A. Konoplyannikov⁴³ , P. Kopciwicz^{39,48} , P. Koppenburg³⁷ , M. Korolev⁴³ ,
659 I. Kostyuk³⁷ , O. Kot⁵², S. Kotriakhova , A. Kozachuk⁴³ , P. Kravchenko⁴³ ,
660 L. Kravchuk⁴³ , M. Kreps⁵⁶ , P. Krokovny⁴³ , W. Krupa⁶⁸ , W. Krzemien⁴¹ ,
661 O.K. Kshyvanskyi⁵², S. Kubis⁷⁹ , M. Kucharczyk⁴⁰ , V. Kudryavtsev⁴³ , E. Kulikova⁴³ ,
662 A. Kupsc⁸¹ , B. K. Kutsenko¹³ , D. Lacarrere⁴⁸ , P. Laguarda Gonzalez⁴⁵ , A. Lai³¹ ,
663 A. Lampis³¹ , D. Lancierini⁵⁵ , C. Landesa Gomez⁴⁶ , J.J. Lane¹ , R. Lane⁵⁴ ,
664 G. Lanfranchi²⁷ , C. Langenbruch²¹ , J. Langer¹⁹ , O. Lantwin⁴³ , T. Latham⁵⁶ ,
665 F. Lazzari^{34,r} , C. Lazzeroni⁵³ , R. Le Gac¹³ , H. Lee⁶⁰ , R. Lefevre¹¹ , A. Leflat⁴³ ,
666 S. Legotin⁴³ , M. Lehuraux⁵⁶ , E. Lemos Cid⁴⁸ , O. Leroy¹³ , T. Lesiak⁴⁰ , E. Lesser⁴⁸,
667 B. Leverington²¹ , A. Li^{4,b} , C. Li¹³ , H. Li⁷¹ , K. Li⁸ , L. Li⁶² , M. Li⁸, P. Li⁷ ,
668 P.-R. Li⁷² , Q. Li^{5,7} , S. Li⁸ , T. Li^{5,d} , T. Li⁷¹ , Y. Li⁸, Y. Li⁵ , Z. Lian^{4,b} ,
669 X. Liang⁶⁸ , S. Libralon⁴⁷ , C. Lin⁷ , T. Lin⁵⁷ , R. Lindner⁴⁸ , V. Lisovskyi⁴⁹ ,
670 R. Litvinov^{31,48} , F. L. Liu¹ , G. Liu⁷¹ , K. Liu⁷² , S. Liu^{5,7} , W. Liu⁸, Y. Liu⁵⁸ ,
671 Y. Liu⁷², Y. L. Liu⁶¹ , A. Lobo Salvia⁴⁵ , A. Loi³¹ , J. Lomba Castro⁴⁶ , T. Long⁵⁵ ,
672 J.H. Lopes³ , A. Lopez Huertas⁴⁵ , S. López Soliño⁴⁶ , Q. Lu¹⁵ , C. Lucarelli²⁶ ,
673 D. Lucchesi^{32,o} , M. Lucio Martinez⁷⁸ , V. Lukashenko^{37,52} , Y. Luo⁶ , A. Lupato^{32,h} ,
674 E. Luppi^{25,k} , K. Lynch²² , X.-R. Lyu⁷ , G. M. Ma^{4,b} , R. Ma⁷ , S. Maccolini¹⁹ ,
675 F. Machefert¹⁴ , F. Maciuc⁴² , B. Mack⁶⁸ , I. Mackay⁶³ , L. M. Mackey⁶⁸ ,
676 L.R. Madhan Mohan⁵⁵ , M. J. Madurai⁵³ , A. Maevskiy⁴³ , D. Magdalinski³⁷ ,
677 D. Maisuzenko⁴³ , M.W. Majewski³⁹, J.J. Malczewski⁴⁰ , S. Malde⁶³ , L. Malentacca⁴⁸,
678 A. Malinin⁴³ , T. Maltsev⁴³ , G. Manca^{31,j} , G. Mancinelli¹³ , C. Mancuso^{29,14,m} ,
679 R. Manera Escalero⁴⁵ , D. Manuzzi²⁴ , D. Marangotto^{29,m} , J.F. Marchand¹⁰ ,
680 R. Marchevski⁴⁹ , U. Marconi²⁴ , E. Mariani¹⁶, S. Mariani⁴⁸ , C. Marin Benito⁴⁵ ,
681 J. Marks²¹ , A.M. Marshall⁵⁴ , L. Martel⁶³ , G. Martelli^{33,p} , G. Martellotti³⁵ ,
682 L. Martinazzoli⁴⁸ , M. Martinelli^{30,n} , D. Martinez Santos⁴⁶ , F. Martinez Vidal⁴⁷ ,
683 A. Massafferri² , R. Matev⁴⁸ , A. Mathad⁴⁸ , V. Matiunin⁴³ , C. Matteuzzi⁶⁸ ,
684 K.R. Mattioli¹⁵ , A. Mauri⁶¹ , E. Maurice¹⁵ , J. Mauricio⁴⁵ , P. Mayencourt⁴⁹ ,
685 J. Mazorra de Cos⁴⁷ , M. Mazurek⁴¹ , M. McCann⁶¹ , L. Mcconnell²² ,
686 T.H. McGrath⁶² , N.T. McHugh⁵⁹ , A. McNab⁶² , R. McNulty²² , B. Meadows⁶⁵ ,
687 G. Meier¹⁹ , D. Melnychuk⁴¹ , F. M. Meng^{4,b} , M. Merk^{37,78} , A. Merli⁴⁹ ,
688 L. Meyer Garcia⁶⁶ , D. Miao^{5,7} , H. Miao⁷ , M. Mikhasenko⁷⁵ , D.A. Milanes⁷⁴ ,
689 A. Minotti^{30,n} , E. Minucci⁶⁸ , T. Miralles¹¹ , B. Mitreska¹⁹ , D.S. Mitzel¹⁹ ,
690 A. Modak⁵⁷ , R.A. Mohammed⁶³ , R.D. Moise¹⁷ , S. Mokhnenko⁴³ , E.
691 F. Molina Cardenas⁸² , T. Mombächer⁴⁸ , M. Monk^{56,1} , S. Monteil¹¹ ,
692 A. Morcillo Gomez⁴⁶ , G. Morello²⁷ , M.J. Morello^{34,q} , M.P. Morgenthaler²¹ ,
693 J. Moron³⁹ , A.B. Morris⁴⁸ , A.G. Morris¹³ , R. Mountain⁶⁸ , H. Mu^{4,b} , Z. M. Mu⁶ ,
694 E. Muhammad⁵⁶ , F. Muheim⁵⁸ , M. Mulder⁷⁷ , K. Müller⁵⁰ , F. Muñoz-Rojas⁹ ,
695 R. Murta⁶¹ , P. Naik⁶⁰ , T. Nakada⁴⁹ , R. Nandakumar⁵⁷ , T. Namut⁴⁸ , I. Nasteva³ ,
696 M. Needham⁵⁸ , N. Neri^{29,m} , S. Neubert¹⁸ , N. Neufeld⁴⁸ , P. Neustroev⁴³,
697 J. Nicolini^{19,14} , D. Nicotra⁷⁸ , E.M. Niel⁴⁹ , N. Nikitin⁴³ , P. Nogarolli³ ,
698 P. Nogga¹⁸ , C. Normand⁵⁴ , J. Novoa Fernandez⁴⁶ , G. Nowak⁶⁵ , C. Nunez⁸² , H. N.
699 Nur⁵⁹ , A. Oblakowska-Mucha³⁹ , V. Obratsov⁴³ , T. Oeser¹⁷ , S. Okamura^{25,k} ,
700 A. Okhotnikov⁴³, O. Okhrimenko⁵² , R. Oldeman^{31,j} , F. Oliva⁵⁸ , M. Olocco¹⁹ ,
701 C.J.G. Onderwater⁷⁸ , R.H. O'Neil⁵⁸ , D. Osthus¹⁹, J.M. Otalora Goicochea³ ,
702 P. Owen⁵⁰ , A. Oyanguren⁴⁷ , O. Ozcelik⁵⁸ , F. Paciolla^{34,u} , A. Padee⁴¹ ,

703 K.O. Padeken¹⁸ , B. Pagare⁵⁶ , P.R. Pais²¹ , T. Pajero⁴⁸ , A. Palano²³ ,
704 M. Palutan²⁷ , G. Panshin⁴³ , L. Paolucci⁵⁶ , A. Papanestis^{57,48} , M. Pappagallo^{23,g} ,
705 L.L. Pappalardo^{25,k} , C. Pappenheimer⁶⁵ , C. Parkes⁶² , B. Passalacqua²⁵ ,
706 G. Passaleva²⁶ , D. Passaro^{34,q} , A. Pastore²³ , M. Patel⁶¹ , J. Patoc⁶³ ,
707 C. Patrignani^{24,i} , A. Paul⁶⁸ , C.J. Pawley⁷⁸ , A. Pellegrino³⁷ , J. Peng^{5,7} ,
708 M. Pepe Altarelli²⁷ , S. Perazzini²⁴ , D. Pereima⁴³ , H. Pereira Da Costa⁶⁷ ,
709 A. Pereiro Castro⁴⁶ , P. Perret¹¹ , A. Perro⁴⁸ , K. Petridis⁵⁴ , A. Petrolini^{28,l} , J. P.
710 Pfaller⁶⁵ , H. Pham⁶⁸ , L. Pica^{34,q} , M. Piccini³³ , L. Piccolo³¹ , B. Pietrzyk¹⁰ ,
711 G. Pietrzyk¹⁴ , D. Pinci³⁵ , F. Pisani⁴⁸ , M. Pizzichemi^{30,n,48} , V. Placinta⁴² ,
712 M. Plo Casasus⁴⁶ , T. Poeschl⁴⁸ , F. Polci^{16,48} , M. Poli Lener²⁷ , A. Poluektov¹³ ,
713 N. Polukhina⁴³ , I. Polyakov⁴³ , E. Polcarpo³ , S. Ponce⁴⁸ , D. Popov⁷ ,
714 S. Poslavskii⁴³ , K. Prasanth⁵⁸ , C. Prouve⁴⁶ , D. Provenzano^{31,j} , V. Pugatch⁵² ,
715 G. Punzi^{34,r} , S. Qasim⁵⁰ , Q. Q. Qian⁶ , W. Qian⁷ , N. Qin^{4,b} , S. Qu^{4,b} ,
716 R. Quagliani⁴⁸ , R.I. Rabadan Trejo⁵⁶ , J.H. Rademacker⁵⁴ , M. Rama³⁴ , M.
717 Ramírez García⁸² , V. Ramos De Oliveira⁶⁹ , M. Ramos Pernas⁵⁶ , M.S. Rangel³ ,
718 F. Ratnikov⁴³ , G. Raven³⁸ , M. Rebollo De Miguel⁴⁷ , F. Redi^{29,h} , J. Reich⁵⁴ ,
719 F. Reiss⁶² , Z. Ren⁷ , P.K. Resmi⁶³ , R. Ribatti⁴⁹ , G. R. Ricart^{15,12} ,
720 D. Riccardi^{34,q} , S. Ricciardi⁵⁷ , K. Richardson⁶⁴ , M. Richardson-Slipper⁵⁸ ,
721 K. Rinnert⁶⁰ , P. Robbe¹⁴ , G. Robertson⁵⁹ , E. Rodrigues⁶⁰ ,
722 E. Rodriguez Fernandez⁴⁶ , J.A. Rodriguez Lopez⁷⁴ , E. Rodriguez Rodriguez⁴⁶ ,
723 J. Roensch¹⁹ , A. Rogachev⁴³ , A. Rogovskiy⁵⁷ , D.L. Rolf⁴⁸ , P. Roloff⁴⁸ ,
724 V. Romanovskiy⁶⁵ , M. Romero Lamas⁴⁶ , A. Romero Vidal⁴⁶ , G. Romolini²⁵ ,
725 F. Ronchetti⁴⁹ , T. Rong⁶ , M. Rotondo²⁷ , S. R. Roy²¹ , M.S. Rudolph⁶⁸ ,
726 M. Ruiz Diaz²¹ , R.A. Ruiz Fernandez⁴⁶ , J. Ruiz Vidal^{81,y} , A. Ryzhikov⁴³ ,
727 J. Ryzka³⁹ , J. J. Saavedra-Arias⁹ , J.J. Saborido Silva⁴⁶ , R. Sadek¹⁵ , N. Sagidova⁴³ ,
728 D. Sahoo⁷⁶ , N. Sahoo⁵³ , B. Saitta^{31,j} , M. Salomoni^{30,48,n} , I. Sanderswood⁴⁷ ,
729 R. Santacesaria³⁵ , C. Santamarina Rios⁴⁶ , M. Santimaria^{27,48} , L. Santoro² ,
730 E. Santovetti³⁶ , A. Saputi^{25,48} , D. Saranin⁴³ , A. Sarnatskiy⁷⁷ , G. Sarpis⁵⁸ ,
731 M. Sarpis⁶² , C. Satriano^{35,s} , A. Satta³⁶ , M. Saur⁶ , D. Savrina⁴³ , H. Szak¹⁷ ,
732 F. Sborzacchi^{48,27} , L.G. Scantlebury Smead⁶³ , A. Scarabotto¹⁹ , S. Schael¹⁷ ,
733 S. Scherl⁶⁰ , M. Schiller⁵⁹ , H. Schindler⁴⁸ , M. Schmelling²⁰ , B. Schmidt⁴⁸ ,
734 S. Schmitt¹⁷ , H. Schmitz¹⁸ , O. Schneider⁴⁹ , A. Schopper⁴⁸ , N. Schulte¹⁹ ,
735 S. Schulte⁴⁹ , M.H. Schune¹⁴ , R. Schwemmer⁴⁸ , G. Schwering¹⁷ , B. Sciascia²⁷ ,
736 A. Sciuccati⁴⁸ , S. Sellam⁴⁶ , A. Semennikov⁴³ , T. Senger⁵⁰ , M. Senghi Soares³⁸ ,
737 A. Sergi^{28,l,48} , N. Serra⁵⁰ , L. Sestini³² , A. Seuthe¹⁹ , Y. Shang⁶ , D.M. Shangase⁸² ,
738 M. Shapkin⁴³ , R. S. Sharma⁶⁸ , I. Shchemerov⁴³ , L. Shchutska⁴⁹ , T. Shears⁶⁰ ,
739 L. Shekhtman⁴³ , Z. Shen⁶ , S. Sheng^{5,7} , V. Shevchenko⁴³ , B. Shi⁷ , Q. Shi⁷ ,
740 Y. Shimizu¹⁴ , E. Shmanin²⁴ , R. Shorkin⁴³ , J.D. Shupperd⁶⁸ , R. Silva Coutinho⁶⁸ ,
741 G. Simi^{32,o} , S. Simone^{23,g} , N. Skidmore⁵⁶ , T. Skwarnicki⁶⁸ , M.W. Slater⁵³ ,
742 J.C. Smallwood⁶³ , E. Smith⁶⁴ , K. Smith⁶⁷ , M. Smith⁶¹ , A. Snoch³⁷ ,
743 L. Soares Lavra⁵⁸ , M.D. Sokoloff⁶⁵ , F.J.P. Soler⁵⁹ , A. Solomin^{43,54} , A. Solovev⁴³ ,
744 I. Solovyev⁴³ , R. Song¹ , Y. Song⁴⁹ , Y. Song^{4,b} , Y. S. Song⁶ ,
745 F.L. Souza De Almeida⁶⁸ , B. Souza De Paula³ , E. Spadaro Norella^{28,l} , E. Spedicato²⁴ ,
746 J.G. Speer¹⁹ , E. Spiridenkov⁴³ , P. Spradlin⁵⁹ , V. Sriskaran⁴⁸ , F. Stagni⁴⁸ ,
747 M. Stahl⁴⁸ , S. Stahl⁴⁸ , S. Stanislaus⁶³ , E.N. Stein⁴⁸ , O. Steinkamp⁵⁰ ,
748 O. Stenyakin⁴³ , H. Stevens¹⁹ , D. Strelalina⁴³ , Y. Su⁷ , F. Suljik⁶³ , J. Sun³¹ ,
749 L. Sun⁷³ , Y. Sun⁶⁶ , D. Sundfeld² , W. Sutcliffe⁵⁰ , P.N. Swallow⁵³ , K. Swientek³⁹ ,
750 F. Swystun⁵⁵ , A. Szabelski⁴¹ , T. Szumlak³⁹ , Y. Tan^{4,b} , M.D. Tat⁶³ ,
751 A. Terentev⁴³ , F. Terzuoli^{34,u,48} , F. Teubert⁴⁸ , E. Thomas⁴⁸ , D.J.D. Thompson⁵³ ,
752 H. Tilquin⁶¹ , V. Tisserand¹¹ , S. T'Jampens¹⁰ , M. Tobin^{5,48} , L. Tomassetti^{25,k} ,

753 G. Tonani^{29,m,48} , X. Tong⁶ , D. Torres Machado² , L. Toscano¹⁹ , D.Y. Tou^{4,b} ,
 754 C. Trippl⁴⁴ , G. Tuci²¹ , N. Tuning³⁷ , L.H. Uecker²¹ , A. Ukleja³⁹ ,
 755 D.J. Unverzagt²¹ , E. Ursov⁴³ , A. Usachov³⁸ , A. Ustyuzhanin⁴³ , U. Uwer²¹ ,
 756 V. Vagnoni²⁴ , V. Valcarce Cadenas⁴⁶ , G. Valenti²⁴ , N. Valls Canudas⁴⁸ ,
 757 H. Van Hecke⁶⁷ , E. van Herwijnen⁶¹ , C.B. Van Hulse^{46,w} , R. Van Laak⁴⁹ ,
 758 M. van Veghel³⁷ , G. Vasquez⁵⁰ , R. Vazquez Gomez⁴⁵ , P. Vazquez Regueiro⁴⁶ ,
 759 C. Vázquez Sierra⁴⁶ , S. Vecchi²⁵ , J.J. Velthuis⁵⁴ , M. Veltri^{26,v} , A. Venkateswaran⁴⁹ ,
 760 M. Verdoglia³¹ , M. Vesterinen⁵⁶ , D. Vico Benet⁶³ , P. V. Vidrier Villalba⁴⁵,
 761 M. Vieites Diaz⁴⁸ , X. Vilasis-Cardona⁴⁴ , E. Vilella Figueras⁶⁰ , A. Villa²⁴ ,
 762 P. Vincent¹⁶ , F.C. Volle⁵³ , D. vom Bruch¹³ , N. Voropaev⁴³ , K. Vos⁷⁸ ,
 763 G. Vouters¹⁰ , C. Vrahas⁵⁸ , J. Wagner¹⁹ , J. Walsh³⁴ , E.J. Walton^{1,56} , G. Wan⁶ ,
 764 C. Wang²¹ , G. Wang⁸ , J. Wang⁶ , J. Wang⁵ , J. Wang^{4,b} , J. Wang⁷³ ,
 765 M. Wang²⁹ , N. W. Wang⁷ , R. Wang⁵⁴ , X. Wang⁸, X. Wang⁷¹ , X. W. Wang⁶¹ ,
 766 Y. Wang⁶ , Z. Wang¹⁴ , Z. Wang^{4,b} , Z. Wang²⁹ , J.A. Ward^{56,1} , M. Waterlaet⁴⁸,
 767 N.K. Watson⁵³ , D. Websdale⁶¹ , Y. Wei⁶ , J. Wendel⁸⁰ , B.D.C. Westhenry⁵⁴ ,
 768 C. White⁵⁵ , M. Whitehead⁵⁹ , E. Whiter⁵³ , A.R. Wiederhold⁶² , D. Wiedner¹⁹ ,
 769 G. Wilkinson⁶³ , M.K. Wilkinson⁶⁵ , M. Williams⁶⁴ , M.R.J. Williams⁵⁸ ,
 770 R. Williams⁵⁵ , Z. Williams⁵⁴ , F.F. Wilson⁵⁷ , M. Winn¹², W. Wislicki⁴¹ ,
 771 M. Witek⁴⁰ , L. Witola²¹ , G. Wormser¹⁴ , S.A. Wotton⁵⁵ , H. Wu⁶⁸ , J. Wu⁸ ,
 772 Y. Wu⁶ , Z. Wu⁷ , K. Wyllie⁴⁸ , S. Xian⁷¹, Z. Xiang⁵ , Y. Xie⁸ , A. Xu³⁴ , J. Xu⁷ ,
 773 L. Xu^{4,b} , L. Xu^{4,b} , M. Xu⁵⁶ , Z. Xu⁴⁸ , Z. Xu⁷ , Z. Xu⁵ , D. Yang⁴ , K. Yang⁶¹ ,
 774 S. Yang⁷ , X. Yang⁶ , Y. Yang^{28,l} , Z. Yang⁶ , Z. Yang⁶⁶ , V. Yeroshenko¹⁴ ,
 775 H. Yeung⁶² , H. Yin⁸ , X. Yin⁷ , C. Y. Yu⁶ , J. Yu⁷⁰ , X. Yuan⁵ , Y. Yuan^{5,7} ,
 776 E. Zaffaroni⁴⁹ , M. Zavertyaev²⁰ , M. Zdybal⁴⁰ , F. Zenesini^{24,i} , C. Zeng^{5,7} ,
 777 M. Zeng^{4,b} , C. Zhang⁶ , D. Zhang⁸ , J. Zhang⁷ , L. Zhang^{4,b} , S. Zhang⁷⁰ ,
 778 S. Zhang⁶³ , Y. Zhang⁶ , Y. Z. Zhang^{4,b} , Y. Zhao²¹ , A. Zharkova⁴³ ,
 779 A. Zhelezov²¹ , S. Z. Zheng⁶ , X. Z. Zheng^{4,b} , Y. Zheng⁷ , T. Zhou⁶ , X. Zhou⁸ ,
 780 Y. Zhou⁷ , V. Zhovkovska⁵⁶ , L. Z. Zhu⁷ , X. Zhu^{4,b} , X. Zhu⁸ , V. Zhukov¹⁷ ,
 781 J. Zhuo⁴⁷ , Q. Zou^{5,7} , D. Zuliani^{32,o} , G. Zunica⁴⁹ .

782 ¹*School of Physics and Astronomy, Monash University, Melbourne, Australia*

783 ²*Centro Brasileiro de Pesquisas Físicas (CBPF), Rio de Janeiro, Brazil*

784 ³*Universidade Federal do Rio de Janeiro (UFRJ), Rio de Janeiro, Brazil*

785 ⁴*Department of Engineering Physics, Tsinghua University, Beijing, China, Beijing, China*

786 ⁵*Institute Of High Energy Physics (IHEP), Beijing, China*

787 ⁶*School of Physics State Key Laboratory of Nuclear Physics and Technology, Peking University, Beijing, China*

789 ⁷*University of Chinese Academy of Sciences, Beijing, China*

790 ⁸*Institute of Particle Physics, Central China Normal University, Wuhan, Hubei, China*

791 ⁹*Consejo Nacional de Rectores (CONARE), San Jose, Costa Rica*

792 ¹⁰*Université Savoie Mont Blanc, CNRS, IN2P3-LAPP, Annecy, France*

793 ¹¹*Université Clermont Auvergne, CNRS/IN2P3, LPC, Clermont-Ferrand, France*

794 ¹²*Département de Physique Nucléaire (DPhN), Gif-Sur-Yvette, France*

795 ¹³*Aix Marseille Univ, CNRS/IN2P3, CPPM, Marseille, France*

796 ¹⁴*Université Paris-Saclay, CNRS/IN2P3, IJCLab, Orsay, France*

797 ¹⁵*Laboratoire Leprince-Ringuet, CNRS/IN2P3, Ecole Polytechnique, Institut Polytechnique de Paris, Palaiseau, France*

799 ¹⁶*LPNHE, Sorbonne Université, Paris Diderot Sorbonne Paris Cité, CNRS/IN2P3, Paris, France*

800 ¹⁷*I. Physikalisches Institut, RWTH Aachen University, Aachen, Germany*

801 ¹⁸*Universität Bonn - Helmholtz-Institut für Strahlen und Kernphysik, Bonn, Germany*

802 ¹⁹*Fakultät Physik, Technische Universität Dortmund, Dortmund, Germany*

803 ²⁰*Max-Planck-Institut für Kernphysik (MPIK), Heidelberg, Germany*

804 ²¹*Physikalisches Institut, Ruprecht-Karls-Universität Heidelberg, Heidelberg, Germany*

805 ²²*School of Physics, University College Dublin, Dublin, Ireland*
806 ²³*INFN Sezione di Bari, Bari, Italy*
807 ²⁴*INFN Sezione di Bologna, Bologna, Italy*
808 ²⁵*INFN Sezione di Ferrara, Ferrara, Italy*
809 ²⁶*INFN Sezione di Firenze, Firenze, Italy*
810 ²⁷*INFN Laboratori Nazionali di Frascati, Frascati, Italy*
811 ²⁸*INFN Sezione di Genova, Genova, Italy*
812 ²⁹*INFN Sezione di Milano, Milano, Italy*
813 ³⁰*INFN Sezione di Milano-Bicocca, Milano, Italy*
814 ³¹*INFN Sezione di Cagliari, Monserrato, Italy*
815 ³²*INFN Sezione di Padova, Padova, Italy*
816 ³³*INFN Sezione di Perugia, Perugia, Italy*
817 ³⁴*INFN Sezione di Pisa, Pisa, Italy*
818 ³⁵*INFN Sezione di Roma La Sapienza, Roma, Italy*
819 ³⁶*INFN Sezione di Roma Tor Vergata, Roma, Italy*
820 ³⁷*Nikhef National Institute for Subatomic Physics, Amsterdam, Netherlands*
821 ³⁸*Nikhef National Institute for Subatomic Physics and VU University Amsterdam, Amsterdam,*
822 *Netherlands*
823 ³⁹*AGH - University of Krakow, Faculty of Physics and Applied Computer Science, Kraków, Poland*
824 ⁴⁰*Henryk Niewodniczanski Institute of Nuclear Physics Polish Academy of Sciences, Kraków, Poland*
825 ⁴¹*National Center for Nuclear Research (NCBJ), Warsaw, Poland*
826 ⁴²*Horia Hulubei National Institute of Physics and Nuclear Engineering, Bucharest-Magurele, Romania*
827 ⁴³*Affiliated with an institute covered by a cooperation agreement with CERN*
828 ⁴⁴*DS4DS, La Salle, Universitat Ramon Llull, Barcelona, Spain*
829 ⁴⁵*ICCUB, Universitat de Barcelona, Barcelona, Spain*
830 ⁴⁶*Instituto Galego de Física de Altas Enerxías (IGFAE), Universidade de Santiago de Compostela,*
831 *Santiago de Compostela, Spain*
832 ⁴⁷*Instituto de Física Corpuscular, Centro Mixto Universidad de Valencia - CSIC, Valencia, Spain*
833 ⁴⁸*European Organization for Nuclear Research (CERN), Geneva, Switzerland*
834 ⁴⁹*Institute of Physics, Ecole Polytechnique Fédérale de Lausanne (EPFL), Lausanne, Switzerland*
835 ⁵⁰*Physik-Institut, Universität Zürich, Zürich, Switzerland*
836 ⁵¹*NSC Kharkiv Institute of Physics and Technology (NSC KIPT), Kharkiv, Ukraine*
837 ⁵²*Institute for Nuclear Research of the National Academy of Sciences (KINR), Kyiv, Ukraine*
838 ⁵³*School of Physics and Astronomy, University of Birmingham, Birmingham, United Kingdom*
839 ⁵⁴*H.H. Wills Physics Laboratory, University of Bristol, Bristol, United Kingdom*
840 ⁵⁵*Cavendish Laboratory, University of Cambridge, Cambridge, United Kingdom*
841 ⁵⁶*Department of Physics, University of Warwick, Coventry, United Kingdom*
842 ⁵⁷*STFC Rutherford Appleton Laboratory, Didcot, United Kingdom*
843 ⁵⁸*School of Physics and Astronomy, University of Edinburgh, Edinburgh, United Kingdom*
844 ⁵⁹*School of Physics and Astronomy, University of Glasgow, Glasgow, United Kingdom*
845 ⁶⁰*Oliver Lodge Laboratory, University of Liverpool, Liverpool, United Kingdom*
846 ⁶¹*Imperial College London, London, United Kingdom*
847 ⁶²*Department of Physics and Astronomy, University of Manchester, Manchester, United Kingdom*
848 ⁶³*Department of Physics, University of Oxford, Oxford, United Kingdom*
849 ⁶⁴*Massachusetts Institute of Technology, Cambridge, MA, United States*
850 ⁶⁵*University of Cincinnati, Cincinnati, OH, United States*
851 ⁶⁶*University of Maryland, College Park, MD, United States*
852 ⁶⁷*Los Alamos National Laboratory (LANL), Los Alamos, NM, United States*
853 ⁶⁸*Syracuse University, Syracuse, NY, United States*
854 ⁶⁹*Pontifícia Universidade Católica do Rio de Janeiro (PUC-Rio), Rio de Janeiro, Brazil, associated to ³*
855 ⁷⁰*School of Physics and Electronics, Hunan University, Changsha City, China, associated to ⁸*
856 ⁷¹*Guangdong Provincial Key Laboratory of Nuclear Science, Guangdong-Hong Kong Joint Laboratory of*
857 *Quantum Matter, Institute of Quantum Matter, South China Normal University, Guangzhou, China,*
858 *associated to ⁴*
859 ⁷²*Lanzhou University, Lanzhou, China, associated to ⁵*
860 ⁷³*School of Physics and Technology, Wuhan University, Wuhan, China, associated to ⁴*

861 ⁷⁴ *Departamento de Física , Universidad Nacional de Colombia, Bogota, Colombia, associated to* ¹⁶
862 ⁷⁵ *Ruhr Universitaet Bochum, Fakultaet f. Physik und Astronomie, Bochum, Germany, associated to* ¹⁹
863 ⁷⁶ *Eotvos Lorand University, Budapest, Hungary, associated to* ⁴⁸
864 ⁷⁷ *Van Swinderen Institute, University of Groningen, Groningen, Netherlands, associated to* ³⁷
865 ⁷⁸ *Universiteit Maastricht, Maastricht, Netherlands, associated to* ³⁷
866 ⁷⁹ *Tadeusz Kosciuszko Cracow University of Technology, Cracow, Poland, associated to* ⁴⁰
867 ⁸⁰ *Universidad da Coruña, A Coruña, Spain, associated to* ⁴⁴
868 ⁸¹ *Department of Physics and Astronomy, Uppsala University, Uppsala, Sweden, associated to* ⁵⁹
869 ⁸² *University of Michigan, Ann Arbor, MI, United States, associated to* ⁶⁸

870 ^a *Centro Federal de Educacão Tecnológica Celso Suckow da Fonseca, Rio De Janeiro, Brazil*

871 ^b *Center for High Energy Physics, Tsinghua University, Beijing, China*

872 ^c *Hangzhou Institute for Advanced Study, UCAS, Hangzhou, China*

873 ^d *School of Physics and Electronics, Henan University , Kaifeng, China*

874 ^e *LIP6, Sorbonne Université, Paris, France*

875 ^f *Universidad Nacional Autónoma de Honduras, Tegucigalpa, Honduras*

876 ^g *Università di Bari, Bari, Italy*

877 ^h *Università di Bergamo, Bergamo, Italy*

878 ⁱ *Università di Bologna, Bologna, Italy*

879 ^j *Università di Cagliari, Cagliari, Italy*

880 ^k *Università di Ferrara, Ferrara, Italy*

881 ^l *Università di Genova, Genova, Italy*

882 ^m *Università degli Studi di Milano, Milano, Italy*

883 ⁿ *Università degli Studi di Milano-Bicocca, Milano, Italy*

884 ^o *Università di Padova, Padova, Italy*

885 ^p *Università di Perugia, Perugia, Italy*

886 ^q *Scuola Normale Superiore, Pisa, Italy*

887 ^r *Università di Pisa, Pisa, Italy*

888 ^s *Università della Basilicata, Potenza, Italy*

889 ^t *Università di Roma Tor Vergata, Roma, Italy*

890 ^u *Università di Siena, Siena, Italy*

891 ^v *Università di Urbino, Urbino, Italy*

892 ^w *Universidad de Alcalá, Alcalá de Henares , Spain*

893 ^x *Facultad de Ciencias Fisicas, Madrid, Spain*

894 ^y *Department of Physics/Division of Particle Physics, Lund, Sweden*

895 [†] *Deceased*